Advanced Waveforms, MAC Design and Dynamic Radio Resource Allocation for Device to-Device in 5G Wireless Networks. Deliverable 1.3: Resource allocation for D2D communications: gain of advanced FBMC

Mylène Pischella, Rostom Zakaria, Didier Le Ruyet, Quentin Bodinier, Faouzi Bader, Hussein Chour

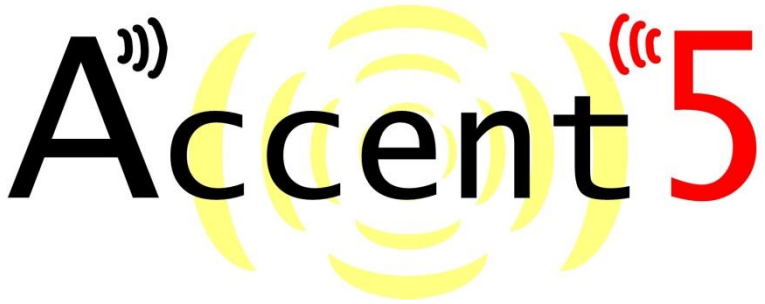

Project acronym: ACCENT5

Project full title: Advanced Waveforms, MAC Design and Dynamic Radio Resource Allocation for Device to-Device in 5G Wireless Networks

N° ANR-14-CE28-0026-01

Deliverable 1.3

Resource allocation for D2D communications: gain of advanced FBMC

Contractual date	T0+33
Actual date	
Version number	1.0

Lead Beneficiary	CNAM, CS
Participants	Mylène Pischella, Rostom Zakaria, Didier le Ruyet (CNAM) Quentin Bodinier, Hussein Chour, Carlos F. Bader (CS)

Estimated person months:	x
Dissemination Level:	PU
Nature:	R
Total number of pages	47

Keywords list: D2D, Coexistence, PSD model, Interferences table, flexible waveforms, 5G, underlay communication.

Executive Summary

Device-to-Device (D2D) communications can be underlaid in cellular networks in order to increase the overall data rates and offload the cellular Base Station from some of the required traffic. In D2D communications, a pair of nearby users directly transmit without passing through the Base Station, which is particularly interesting for devices located at the border of cell. These devices then require low transmit power. Consequently, the same frequency resources can be reused by several D2D pairs that are located far away in the network (and possibly in the same cell), since they generate low interference to each other. D2D pairs are however subject to cellular interference.

In this deliverable, we investigate several techniques to increase the data rates and propose new algorithms to optimize resource allocation in these contexts. We first study the influence of asynchronous interferences on D2D communications. Indeed, in D2D communications, the received interference may be asynchronous with the received useful signal, leading to inter-channel interference (ICI). ICI depends on the waveform that is used for the multi-carrier modulation and is particularly high when using CP-OFDM as in 4G networks, whereas ICI is low with the FBMC-OQAM waveform, which is well localized in the frequency domain. Taking into account ICI and the different waveforms, we propose a distributed power allocation algorithm for underlay asynchronous D2D communications and a distributed Resource Block allocation algorithm that aims at maximizing the average number of multiplexed D2D pairs.
All simulation results show that FBMC-OQAM is far more efficient than CP-OFDM thanks to lower ICI.

ICI can be even more mitigated if a new waveform called COW-CFMC is used. It is particularly robust to time and frequency misalignment. This feature is makes it well-suited for future use in D2D communications.

The data rates results and ICI that are first used in this deliverable assume that both cellular transmission and D2D transmission use the same waveform. However, both types of communications may choose to use different waveforms. For instance, cellular communications could keep using CP-OFDM to be compliant with LTE and LTE-A networks, whereas D2D communications may use more advanced waveforms in order to generate low ICI on cellular communications. We evaluate the influence of the coexistence between cellular communications and D2D communications when different waveforms are used for cellular and D2D communications. The studied waveforms are OFDM, FMT, GFDM, FBMC/OQAM, FBMC-PAM, F-OFDM and UFMC.

Finally, future D2D communications may be even more improved if all devices are equipped with Full Duplex. Devices can then transmit and receive at the same time, but they suffer from self-interference. The ergodic capacity can then be increased by optimizing power allocation, taking into account self-interference. The ergodic capacity improvement thanks to FD depend on the relative location of D2D and of the interference cellular users that share the same frequency resources, as well as on the ability of devices to remove self-interference.

These different scenarios show all the possible benefits brought by D2D communications in underlay communications, whether D2D are subject to asynchronous interference or able to transmit and receive in Full Duplex. A combination of both capabilities would consequently lead to great improvements in the overall cellular and D2D spectral efficiency for future cellular networks. Moreover, the optimization of resource allocation is necessary to achieve great rates improvements.

TABLE OF CONTENTS

EXECUTIVE SUMMARY **3**

1 INTRODUCTION **6**

2 PER-RB RESOURCE ALLOCATION FOR ASYNCHRONOUS D2D COMMUNICATIONS **6**

2.1 SYSTEM MODEL 6
2.2 PER RB ALLOCATION CONSTRAINT 7

3 DISTRIBUTED POWER ALLOCATION ALGORITHM **8**

3.1 POWER ALLOCATION ALGORITHM 8
3.2 NUMERICAL RESULTS 11

4 DISTRIBUTED RESOURCE-BLOCK ALLOCATION ALGORITHM FOR D2D MULTIPLEXING MAXIMIZATION **12**

4.1 D2D MULTIPLEXING OPTIMIZATION PROBLEM 13
4.2 HEURISTIC BASED ON THE INFINITY NORM 14
4.3 SIMULATION RESULTS 15

5 COW-CFMC: A NEW WAVEFORM FOR ASYNCHRONOUS MULTI-USER ACCESS **16**

5.1 REVIEW AND PROPERTIES OF WCP-COQAM 16
5.1.1 Review on WCP-COQAM *16*
5.1.2 Properties of Circular OQAM *17*
5.2 COW-CFMC DESCRIPTION 20
5.3 POWER SPECTRUM DENSITY 22
5.4 ROBUSTNESS TO TIME AND FREQUENCY MISALIGNMENT 24
5.4.1 Timing offset *24*
5.4.2 Carrier frequency offset (CFO) *26*

6 SERVING SPATIALLY CLUSTERED D2D SCENARIOS USING DIFFERENT WAVEFORMS **28**

6.1 SYSTEM MODEL 29
6.1.1 Channel Modelling *29*
6.1.2 Performance Measures *30*
6.2 EVALUATION AND SYSTEM PERFORMANCES 31
6.2.1 Cell Radius *33*
6.2.2 Cluster Radius *34*
6.3 SUMMARY 35

7 OPTIMAL POWER ALLOCATION FOR FULL DUPLEX D2D COMMUNICATION **35**

7.1 SYSTEM MODEL 36
7.2 ERGODIC CAPACITY ANALYSIS 37
7.3 MAXIMIZING THE FULL DUPLEX D2D ERGODIC CAPACITY 38
7.3.1 Analysis of the full duplex rate *39*
7.3.2 The Optimal power allocation scheme *39*
7.4 NUMERICAL RESULTS 40
7.5 MAIN OUTPUTS 42

8 CONCLUSION **43**

9 REFERENCES AND GLOSSARY **44**

9.1 REFERENCES 44
9.2 GLOSSARY 47

LIST OF FIGURES

Figure 1: Weighted sum rate vs number of D2D pairs....12
Figure 2: Weighted sum rate vs I_0, K=32 12
Figure 3: Average number of multiplexed D2D pairs....15
Figure 4: Average data rate depending on the multiplexing technique....16
Figure 5: Spectrum of the M/2-downsampled autocorrelation function of the periodic Mirabbasi-Martin filter $\tilde{g}[m]$ with overlapping factor K=8. 21
Figure 6: Coefficients of the diagonal matrix D_(q,q) for even and odd subcarrier index q using Mirabbasi-Martin filter with overlapping factor K=8. 22
Figure 7: Power Spectrum Density evaluation of different schemes 23
Figure 8: Power Spectrum Density evaluation of different schemes. 24
Figure 9: per-subcarrier NMSE against timing offset (samples). 25
Figure 10: Average NMSE against timing offset (samples). 26
Figure 11: per-subcarrier NMSE against CFO. 27
Figure 12: average NMSE against CFO 28
Figure 13: The box plots of DUE SINR show that a large performance increase can be obtained by choosing an appropriate enhanced waveform. 32
Figure 14: Rate performance of DUEs taking into account bandwidth efficiency. 33
Figure 15: As the cell radius increases, DUE SINR increases and reduction in CUE SINR decreases. 34
Figure 16: Employing an appropriate enhanced waveform for DUEs yields the greatest benefit in small clusters in which inter-DUE leakage interference is most significant. 35
Figure 17: A FD-D2D pair shares the resources of one cellular user, which creates interference between the two types of links. 36
Figure 18: Comparison of FD-D2D rate obtained from the exhaustive search and from the proposed power allocation scheme in the symmetric case 41
Figure 19: Comparison of FD-D2D rate obtained from the exhaustive search and from our proposed power allocation scheme in the asymmetric case 41
Figure 20: The optimal power ratios variation w.r.t to CUE location.(η =-70dB) 42
Figure 21: The effect of the CUE location on the FD rate.(η = -70dB)....42

LIST OF TABLES

Table 1: Bandwidth Efficiency of Waveforms 30
Table 2: Simulation parameters....31

1 Introduction

The wide usage of Device-to-Device (D2D) communications in cellular networks should lead to a large spectral efficiency increase, since frequency spectrum can be reused in D2D communications. However, large gains can only be obtained if interference is handled by resource allocation. Moreover, in D2D communications, the received interference may be asynchronous with the received useful signal, leading to inter-channel interference (ICI). ICI must consequently also be taken into account in resource allocation. In this deliverable, we present a means to include ICI in the data rate expression, so that resource allocation problems can be easily written and solved, while taking into account ICI. We the propose a distributed power allocation algorithm for underlay asynchronous D2D communications and a distributed Resource Block allocation algorithm that aims at maximizing the average number of multiplexed D2D pairs. All algorithms are tested with CP-OFDM and FBMC-OQAM, and show the superiority of FBMC-OQAM in asynchronous transmissions.
We also propose a new waveform called COW-CFMC that is particularly robust to time and frequency misalignment. This feature is makes it well-suited for future use in D2D communications.
Then a complete system-level analysis of the coexistence between cellular communications and D2D communications when different enhanced waveforms are used for cellular and D2D communications is provided. The studied waveforms are OFDM, FMT, GFDM, FBMC/OQAM, FBMC-PAM, F-OFDM and UFMC.
Finally, the last section of this deliverable investigates resource allocation with D2D communications when all devices are able to use Full Duplex (FD). Devices can then transmit and receive at the same time, but they suffer from self-interference. We derive the FD ergodic capacity for D2D transmissions including self-interference, and optimize power allocation in order to maximize the ergodic capacity.

2 Per-RB resource allocation for asynchronous D2D communications

Frequency spectrum reuse is one of the main tools to achieve very large data rates in the cell with D2D communications. The D2D pairs that are located far enough may reuse the same resources while generating low interference level. In underlay D2D communications, the interference at the BS due to D2D transmitters must also be handled. Assuming that D2D pairs have been allocated to Resource Blocks (RB), some co-channel interference may still remain because the number of D2D pairs may be far larger than the number of RB. Moreover, some inter-channel interference (ICI) potentially involving close D2D pairs may be present due to asynchronous transmissions between D2D pairs. In the latter case, using multi-carrier modulations with good spectral localization properties can mitigate this ICI. Interference must consequently be managed by power control. In this section, we propose a RB-level power allocation algorithm. It does take into account ICI through the ICI weight vector that is associated with a given multi-carrier modulation. Even though the ICI weight vector is defined per sub-carrier, the proposed power allocation algorithm is performed per RB.

2.1 System model

We consider K D2D pairs located in one cell. OFDM and FBMC-OQAM multi-carrier techniques with N RBs composed of M adjacent subcarriers are compared. Let $L = M \times N$ be the total number of subcarriers.

All D2D transmitters are synchronous with their receiver, and asynchronous with any other receiver, including the BS. Then, each D2D transmitter's power in RB r generates ICI at the other D2D receivers, not only on the subcarriers of RB r, but also on the subcarriers of the adjacent RBs. The ICI is modelled as interference weights to apply on the power vector $\mathbf{p}$ [11]. Their spread and amplitude depend on the multi-carrier modulation type. Let Δ be the OFDM cyclic prefix (CP) and T the multi-carrier symbol durations. The ICI weights expressions have been derived in [[11]1] for OFDM and FBMC-OQAM, when the timing offset is uniformly distributed in $[0; T + \Delta]$ and $[0; T]$, respectively. Each subcarrier l generates ICI weights on at most D adjacent subcarriers l' on its left and right. D depends on the multi-carrier modulation and is larger with OFDM than with FBMC-OQAM. ICI weights are gathered in vector $\mathbf{V}$ of size L, where $V_{|l-l'|} = 0$ if $|l - l'| > D$.

Let us denote by $\bar{\mathbf{G}}_{kq}$ the $L \times L$ channel gain matrix between the transmitter of the q-th D2D pair and the receiver of the k-th D2D pair. The elements of the matrix $\bar{\mathbf{G}}_{kq}$ are given by:

$$\begin{cases} \bar{\mathbf{G}}_{kq}(i,j) = g_{kq}(j) V_{|i-j|} & \forall k \neq q \\ \bar{\mathbf{G}}_{kk}(i,j) = g_{kk}(j) \delta_{i-j} & \forall k \end{cases} \quad (1)$$

where $g_{kq}(j)$ is the channel gain from the transmitter of pair q to the receiver of pair k in the j-th subcarrier, V_d is the interference coefficient for the spectral distance $d \geq 0$, and δ_x stands for the Kronecker delta. Let $p_q(j)$ be the transmitted

power at the j-th subcarrier by the transmitter q. Then the vector $\bar{\mathbf{y}}_k$ composed of received signal powers $y_k(l)$ at the l-th subcarrier for the k-th receiver, $\forall k \in \{0,\dots,K-1\}$, is:

$$\underbrace{\begin{bmatrix} y_k(0) \\ \vdots \\ y_k(L-1) \end{bmatrix}}_{\bar{\mathbf{y}}_k} = \bar{\mathbf{G}}_{kk} \underbrace{\begin{bmatrix} p_k(0) \\ \vdots \\ p_k(L-1) \end{bmatrix}}_{\bar{\mathbf{p}}_k} + \sum_{\substack{q=0 \\ q\neq k}}^{K-1} \bar{\mathbf{G}}_{kq} \underbrace{\begin{bmatrix} p_q(0) \\ \vdots \\ p_q(L-1) \end{bmatrix}}_{\bar{\mathbf{p}}_q} \tag{2}$$

Let $\tilde{\mathbf{p}} = [\bar{\mathbf{p}}_0^T, \bar{\mathbf{p}}_1^T, \dots, \bar{\mathbf{p}}_{K-1}^T]^T$ and $\mathbf{y} = [\bar{\mathbf{y}}_0^T, \bar{\mathbf{y}}_1^T, \dots, \bar{\mathbf{y}}_{K-1}^T]^T$. Equation (2) can be written as:

$$\mathbf{y} = \underbrace{\begin{bmatrix} \bar{\mathbf{G}}_{00} & \bar{\mathbf{G}}_{01} & & \bar{\mathbf{G}}_{0(K-1)} \\ \bar{\mathbf{G}}_{10} & \bar{\mathbf{G}}_{11} & & \bar{\mathbf{G}}_{1(K-1)} \\ \vdots & & \ddots & \vdots \\ \bar{\mathbf{G}}_{(K-1)0} & \bar{\mathbf{G}}_{(K-1)1} & & \bar{\mathbf{G}}_{(K-1)(L-1)} \end{bmatrix}}_{\tilde{\mathbf{G}}} \tilde{\mathbf{p}} \tag{3}$$

2.2 Per RB allocation constraint

We assume that power allocation is performed at RB level. Consequently, all subcarriers within a single RB have the same allocated power. In this case, the vector of transmit power $\tilde{\mathbf{p}}$ is expressed as:

$$\tilde{\mathbf{p}} = (\mathbf{I}_{KN} \otimes \mathbf{1}_M)\mathbf{p} \tag{4}$$

where $\otimes$ stands for the Kronecker product, $\mathbf{I}_{KN}$ is the identity matrix of size KN, $\mathbf{1}_M$ is a $M \times 1$ vector whose elements are set to 1, and $\mathbf{p}$ is a $KN \times 1$ vector whose entries are the transmit power in each RB. Then eq. (3) becomes:

$$\mathbf{y} = \tilde{\mathbf{G}} \underbrace{(\mathbf{I}_{KN} \otimes \mathbf{1}_M)}_{\mathbf{S}} \mathbf{p} = \mathbf{F}\mathbf{p} \tag{5}$$

where $\mathbf{F} = \tilde{\mathbf{G}}\mathbf{S}$ is a $KL \times KN$ matrix.

Similarly, the interference received by the BS from D2D transmitters is written as:

$$\mathbf{I}_{BS} = \underbrace{[\bar{\mathbf{A}}_0 \quad \bar{\mathbf{A}}]}_{\tilde{\mathbf{A}}} \mathbf{p} = \widetilde{\mathbf{A}\mathbf{S}\mathbf{p}} = \mathbf{A}\mathbf{p} \tag{6}$$

where $\bar{\mathbf{A}}_k$ is a $L \times L$ matrix given by:

$$\bar{\mathbf{A}}_k(i,j) = h_k(\mathrm{j}) V_{|i-j|} \quad \forall k \in \{0,\dots,K-1\}$$

and $h_k(j)$ is the interference channel gain at subcarrier j between the k-th D2D tranmitter and the BS.

The following notations are used in the rest of the deliverable:

- $P_j^r = \mathbf{p}(r + jM)$ is the power allocated for user j in the r-th RB,
- $F_{rj}^{lk} = \mathbf{F}(l + kL, r + jN)$ is the element of matrix $\mathbf{F}$ in line $l + kL$ and row $r + jN$,
- $A_{kr}^{l} = \mathbf{A}(l, r + kN)$ is the interference gain at the BS in subcarrier l from transmitter k and RB r,
- F_{rk}^{lk} is the direct channel between transmitter k and its receiver in subcarrier l,

- $\mathbb{B}_j$ is the set of RB indices used by transmitter j,
- $\mathbb{R}_r$ is the index set of the subcarriers in the r-th RB.

The interference received by user k in subcarrier l I_k^l is then:

$$I_k^l = \sum_{\substack{j=0 \\ j\neq k}}^{K-1} \sum_{r\in\mathbb{B}_j} F_{rj}^{lk} P_j^r$$

The spectral efficiency of user k in RB r is:

$$R_k^r(\mathbf{p}) = \log(1 + \mathrm{SINR}_k^r)$$

Where $\log(x)$ stands for $\log_2(x)$ in order to simplify notations.

3 Distributed power allocation algorithm

In this section, we focus on power allocation and determine a distributed algorithm for maximizing the weighted sum rate, under a high Signal to Interference plus Noise Ratio (SINR) assumption.
We assume that RBs allocation has been performed before power allocation in such a way that interference is low, and the SINR is high. Then the utility function of user k in RB r, defined as his weighted spectral efficiency, is: $u_k^r(\mathbf{p}) = \alpha_k \log(\mathrm{SINR}_k^r)$.

Using the per-RB power constraint the utility function per user k and RB r becomes:

$$u_k^r(\mathbf{p}) = \sum_{l\in\mathbb{R}_r} \alpha_k \log\left(\frac{F_{rk}^{lk} P_k^r}{n_k^l + I_k^l}\right) = = \alpha_k M \log(P_k^r) + \alpha_k \log\left(\prod_{l\in\mathbb{R}_r} \frac{F_{rk}^{lk}}{n_k^l + I_k^l}\right)$$

3.1 Power allocation algorithm

The weighted sum rate maximization problem is written as :

$$\max_{\mathbf{p}\geq 0} \sum_{k=0}^{K-1} \sum_{r\in\mathbb{B}_k} u_k^r(\mathbf{p})$$

$$\text{s.t.} M \sum_{r\in\mathbb{B}_k} P_k^r \leq P_{max} \ \forall k \in \{0,\dots,K-1\} \quad (C1)$$

$$\text{s.t.} \sum_{k=0}^{K-1} \sum_{r\in\mathbb{B}_k} A_{kr}^l P_k^r \leq I_0 \ \forall l \in \{0,\dots,L-1\} \quad (C2)$$

where P_{max} is the maximum transmit power per user and I_0 is the maximum allowed interference per subcarrier at the BS. Since problem (10) belongs to the class of geometric programming [1[12]], it has a unique optimal solution which must satisfy the Karush-Kuhn-Tucker (KKT) conditions. The Lagrangian of this problem is:

$$\mathcal{L}(\mathbf{p}) = \sum_{k=0}^{K-1} \sum_{r \in \mathbb{B}_k} u_k^r(\mathbf{p}) - \sum_{k=0}^{K-1} \mu_k \left(M \sum_{r \in \mathbb{B}_k} P_k^r - P_{max} \right) - \sum_{l=0}^{L-1} \lambda_l \left(\sum_{k=0}^{K-1} \sum_{r \in \mathbb{B}_k} \frac{A_{kr}^l}{I_0} P_k^r - 1 \right)$$

where $\boldsymbol{\mu}$ and $\boldsymbol{\lambda}$ are Lagrange multipliers, that are positive by definition. At the optimal solution $\mathbf{p}^*$, the gradient of the Lagrangian is equal to $\mathbf{0}$. Then there exists unique Lagrange multiplier vectors $\boldsymbol{\mu}^*$ and $\boldsymbol{\lambda}^*$ such that for all k_0 and $r_0 \in \mathbb{B}_{k_0}$:

$$\frac{\alpha_{k_0} M}{P_{k_0}^{r_0 *}} + \sum_{\substack{j=0 \\ j \neq k_0}}^{K-1} \sum_{r \in \mathbb{B}_j} \frac{\partial u_j^r(\mathbf{p}^*)}{\partial P_{k_0}^{r_0}} = \mu_{k_0} M + \sum_{l=0}^{L-1} \frac{A_{k_0 k_0}^l}{I_0} \lambda_l$$

The derivative of utility functions u_j^r with respect to $P_{k_0}^{r_0}$, with $j \neq k_0$, is:

$$\frac{\partial u_j^r(\mathbf{p}^*)}{\partial P_{k_0}^{r_0}} = -\alpha_j \sum_{l \in \mathbb{R}_r} \frac{F_{r_0 k_0}^{lj}}{n_j^l + I_j^l}$$

Consequently, the derivative of the Lagrangian becomes:

$$\frac{\alpha_{k_0} M}{P_{k_0}^{r_0 *}} - \sum_{\substack{j=0 \\ j \neq k_0}}^{K-1} \sum_{r \in \mathbb{B}_j} \sum_{l \in \mathbb{R}_r} \frac{\alpha_j F_{r_0 k_0}^{lj}}{n_j^l + I_j^l} = \mu_{k_0} M + \sum_{l=0}^{L-1} \frac{A_{k_0 r_0}^l}{I_0} \lambda_l$$

And the optimum value of $P_{k_0}^{r_0}$ finally is:

$$P_{k_0}^{r_0 *} = \frac{\alpha_{k_0} M}{f_{k_0}^{r_0}(\mathbf{p}^*, \mu_{k_0}^*, \boldsymbol{\lambda}^*)}$$

with

$$f_{k_0}^{r_0}(\mathbf{p}^*, \mu_{k_0}^*, \boldsymbol{\lambda}^*) = \mu_{k_0}^* M + \sum_{l=0}^{L-1} \frac{A_{k_0 r_0}^l}{I_0} \lambda_l^* + \sum_{\substack{j=0 \\ j \neq k_0}}^{K-1} \sum_{l \in \Omega_j} \frac{\alpha_j F_{r_0 k_0}^{lj}}{n_j^l + I_j^l(\mathbf{p}^*)}$$

where $\Omega_j = \bigcup_{r \in \mathbb{B}_j} \mathbb{R}_r$ is the set of subcarriers allocated to user j.

We now prove that the power allocation algorithm can be implemented in a distributed way. $\boldsymbol{F}$ can be written as:

$$\mathbf{F}(i,j) = \sum_{k=0}^{KL-1} \widetilde{\mathbf{G}}(i,k) \mathbf{S}(k,j) = \sum_{k=jM}^{jM+(M-1)} \widetilde{\mathbf{G}}(i,k)$$

Moreover, since $\mathbf{S}(k,j) = 1$ if $\left\lfloor \frac{k}{j} \right\rfloor = j$ and $\mathbf{S}(k,j) = 0$ elsewhere, with $\lfloor x \rfloor$ the nearest lower integer of x.

Besides, by construction of $\widetilde{\mathbf{G}}$ (see eq. (3)) :

$$\widetilde{\mathbf{G}}(i,k) = \overline{\mathbf{G}}_{\left\lfloor \frac{i}{L} \right\rfloor \left\lfloor \frac{k}{L} \right\rfloor} \left(i - \left\lfloor \frac{i}{L} \right\rfloor L, k - \left\lfloor \frac{k}{L} \right\rfloor L \right)$$

Then $F_{r_0 k_0}^{lj}$ is equal to:

$$F_{r_0 k_0}^{lj} = \mathbf{F}(l + jL, r_0 + k_0 N) = \sum_{p=0}^{M-1} \overline{\mathbf{G}}_{j k_0}(l, r_0 M + p)$$

Using the initial definition (1) of $\overline{\mathbf{G}}$, we finally obtain:

$$F_{r_0 k_0}^{lj} = \sum_{p=0}^{M-1} g_{j k_0}(r_0 M + p) V_{|l - r_0 M - p|} \quad \forall j \neq k_0$$

Afterwards, during the iterative phase, each receiver j transmits interference information $\Pi_j^l(\mathbf{p})$ to the BS on the UL control channel:

$$\Pi_j^l(\mathbf{p}) = \frac{\alpha_j}{n_j^l + I_j^l(\mathbf{p})}$$

The BS then forwards all $\Pi_j^l(\mathbf{p})$ to all D2D transmitters on the DL control channel, along with $\boldsymbol{\lambda}$ if its value has been updated. Transmitter k_0 finally computes $\sum_{l \in \Omega_j} F_{r_0 k_0}^{lj} \Pi_j^l(\mathbf{p})$ in RB r_0 and updates $P_{k_0}^{r_0}$ with (14).

To summarize, the power allocation algorithm is performed as follows: first, at $T = 0$, dual prices $\mu_{k_0}(T)$, $\forall k_0 \in \{0, \ldots, K-1\}$ and $\lambda_{l_0}(T)$, $\forall l_0 \in \{0, \ldots, L-1\}$ are initialized. Then for fixed values of $\boldsymbol{\mu}(T)$ and $\boldsymbol{\lambda}(T)$, an iterative algorithm is used for power allocation, independently on all RB $r_0 \in \{0, \ldots, N-1\}$. $\mathbf{p}$ and $\boldsymbol{\Pi}$ are initialized with equal power allocation.

Then at each iteration $T_i < T_{i,max}$, where $T_{i,max}$ is the maximum number of iterations, all users k_0 active in r_0 perform the following two steps:

- Power update: use eq. (14) with $\mathbf{p}(T_i)$, $\mu_{k_0}(T)$ and $\boldsymbol{\lambda}(T)$ as inputs to compute $\mathbf{p}(T_i + 1)$.
- Interference information update: compute the interference information $\Pi_{k_0}^{l_0}(\mathbf{p}(T_i + 1))$ with:

$$\Pi_{k0}^{l0}(\mathbf{p}(T_i + 1)) = \frac{\alpha_{k0}}{n_{k0}^{l0} + I_{k0}^{l0}(\mathbf{p}(T_i))}$$

At the end of this loop, dual prices are updated as follows, where $\kappa > 0$ and $\delta > 0$ are small positive steps:

$$\mu_{k_0}(T+1) = \left[\mu_{k_0}(T) + \kappa \left(\sum_{r \in \mathbb{B}_{k_0}} M P_{k_0}^r(T_{i,max}) - P_{\max} \right) \right]^+$$

$\forall k_0 \in \{0, \ldots, K-1\}$, where $[a]^+ = \max\{0, a\}$, and

$$\lambda_{l_0}(T+1) = \left[\lambda_{l_0}(T) + \delta \left(\sum_{k=0}^{K-1} \sum_{r \in \mathbb{B}_k} \frac{A_{kr}^{l_0}}{I_0} P_k^r(T_{i,max}) - 1 \right) \right]^+$$

$\forall l_0 \in \{0, \ldots, L-1\}$. This process is repeated $T_{d,max}$ times until convergence.

Similarly to [1[13]], it can be shown that this algorithm converges for small enough values of steps $\kappa > 0$ are $\delta > 0$. Since the fixed point of the iterative algorithm verifies all KKT conditions of problem (10), it is its global optimum.

3.2 Numerical results

Monte-Carlo simulations are conducted with a cell bandwidth $B = 10$ MHz. The Fast Fourier Transform size is 1024. There are $L = 600$ active subcarriers of 15 kHz grouped in $N = 50$ RBs and the cell radius is 500 m with omnidirectional antenna. D2D transmitters' locations follow a uniform distribution in the cell, and each receiver is uniformly located at most at 50 m from its transmitter. P_{max} is equal to 21 dBm and the thermal noise per subcarrier is equal to -132 dBm. Each D2D pair has a uniform random weight between 0 and 1, with $\sum_{k=1}^{K} \alpha_k = 1$. The path loss model is small cells $L_{\mathrm{dB}} = 140 + 36.8\log_{10}(d)$ if the receiver is a device, and LTE urban $L_{\mathrm{dB}} = 128.1 + 37.6\log_{10}(d)$ if the receiver is the BS. The log-normal shadowing has a standard deviation equal to 4 dB for D2D communications and to 9 dB for Device-to-BS interference. Multi-path fading is computed with Indoor Channel-B model [1[14]].

ICI weights are computed using the formula from [[11]1] with OFDM LTE parameters $\Delta = 4.69\mu$s and $T = 66.6\mu$s. Only weights exceeding 10^{-3} are considered. Then D is equal to 9 with OFDM and 1 with FBMC-OQAM. The $D + 1$ non-zero elements of vector $\mathbf{V}$ are equal to:

$$\mathbf{V}_{\mathrm{OFDM}} = [6.89 \times 10^{-1}, 9.47 \times 10^{-2}, 2.37 \times 10^{-2}, 1.05 \times 10^{-2}, 5.9 \times 10^{-3}, 3.8 \times 10^{-3}, 2.6 \times 10^{-3}, 1.9 \times 10^{-3}, 1.5 \times 10^{-3}, 1.12 \times 10^{-3}] \quad (21)$$

$$\mathbf{V}_{\mathrm{FBMC}} = [8.23 \times 10^{-1}, 8.81 \times 10^{-2}] \quad (22)$$

The reference vector is $\mathbf{V}_{\mathrm{PS}} = [1]$ for Perfectly Synchronized (PS) transmission, which represents a theoretical upper-boud with CP $\Delta = 0$.

RB allocation is performed by graph-coloring with DSATUR algorithm [1[15]]: if the distance between transmitter k and receiver k', with $k \neq k'$, is lower than a threshold D_{int}, k and k' belong to different colors. D_{int} is obtained by bisection search to exactly reach 5 colors, whatever the number of D2D pairs in the cell. Then all D2D pairs of color c are multiplexed on RBs l such that $l \bmod(5) = c$. RBs are spread in the bandwidth in order to benefit from frequency diversity.

Fig. 3 shows the performance of our proposed algorithm (called DADP for Dual Asynchronous Distributed Pricing) when constraint $(C2)$ is not taken into account. It is compared with a reference case without power control (called EPA for Equal Power Allocation), where each D2D transmitter equally splits its power on all its allocated RB. Fig. 0 shows the effectiveness of DADP: with FBMC-OQAM, the weighted sum rate with DADP is up to 9.4% higher than that achieved with EPA, which corresponds to an increase of 1.5 Mbits/s. Besides, the weighted sum rate with DADP-FBMC-OQAM is very close to that obtained with DADP-PS (its decrease is at most 2.5%), contrary to OFDM (its decrease reaches 14.8%). This is due to the lower ICI spread of FBMC-OQAM and the CP of OFDM, that generates an overhead of $\Delta/(\Delta + T)$. Fig. 4 represents the weighted sum rate with DADP when $K = 32$ with constraint $(C2)$, when I_0 varies. It is not possible to compare with EPA in this case since EPA would not necessarily fulfill constraint $(C2)$. FBMC-OQAM is still far more efficient than OFDM, and the weighted sum rate with FBMC is less than 1.8% from the upper bound obtained with PS. Moreover, we can notice that D2D data rates are very high, even though they generate low interference level at the BS. This shows that D2D pairs can be efficiently underlaid in cellular networks.

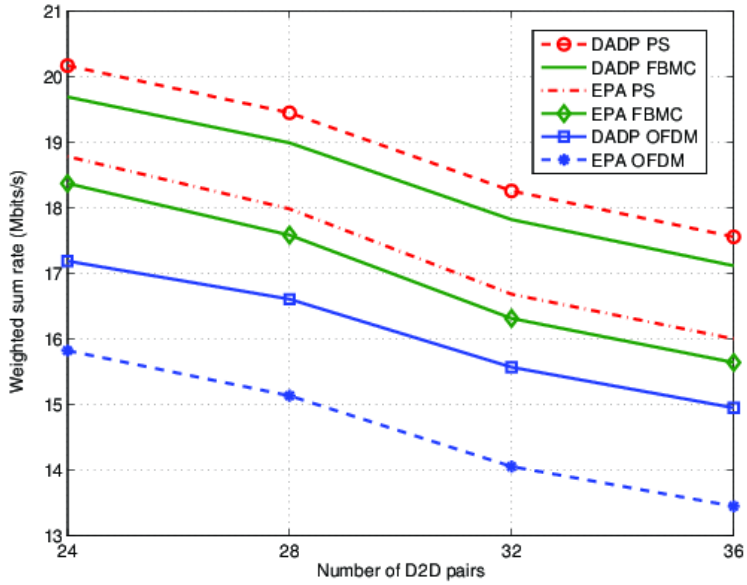

Figure 1: Weighted sum rate vs number of D2D pairs

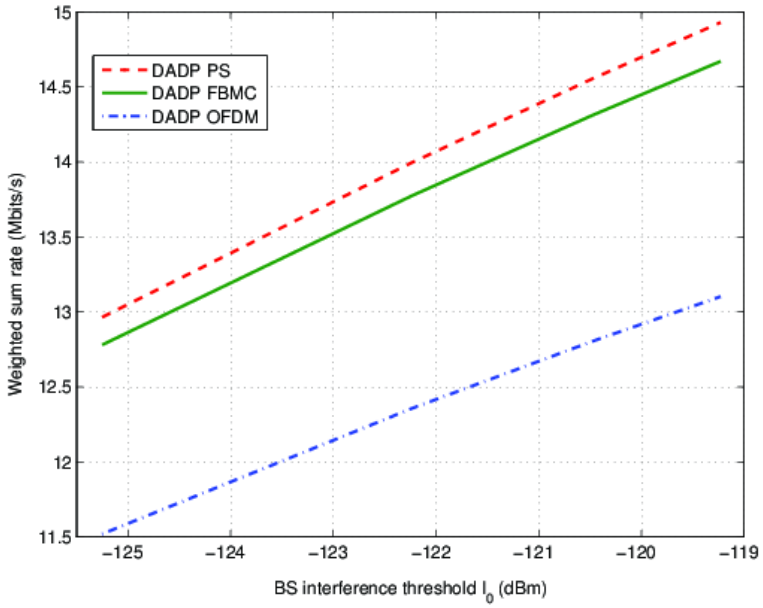

Figure 2: Weighted sum rate vs I_0, K=32

4 Distributed resource-block allocation algorithm for D2D multiplexing maximization

Good performance results, showing the effectiveness of FBMC-OQAM, have been obtained with power allocation.Additional gain can be obtained when RB allocation is optimized as well. In this section, we first present the RB allocation problem and propose a distributed heuristic to solve it.

4.1 D2D multiplexing optimization problem

We consider the multiplexing problem of all K devices on the N RB, with the same system model as in sections 1 and 2, except that we assume that D2D pairs are using a different bandwidth than the cellular users. Consequently, this is an overlay D2D network. The objective, in this section, is to determine the largest set of D2D pairs that can be jointly active. The RB allocation problem then becomes a multiplexing problem. Because of ICI, this problem is not separable per RB, and all RB must be considered jointly.

Let a_k^r be a binary value indicating if D2D pair k is active in RB r. Let γ be the target SINR per subcarrier. If $a_k^r = 1$, then each D2D pair k is active in RB r with its SINR in all subcarriers $l \in \mathbb{R}_r$ is equal to γ. Otherwise, $a_k^r = 0$ and D2D pair is not allocated in RB r. The objective of RB allocation is to determine the vector $\boldsymbol{a}$ that $a(r + kN) = a_k^r$ providing the optimum value of a given optimization problem. Vector $\boldsymbol{a}$ must be optimized considering co-channel and inter-channel interference coming from all interfering D2D pairs.
The SINR condition is written as follows, for $r \in \{0,\dots,N-1\}$, $l \in \mathbb{R}_r$, $\forall\, k \in \{0,\dots,K-1\}$:

$$\frac{F_{rk}^{lk} P_k^r}{n_k^l + \sum_{j=0;j\neq k}^{K-1} \sum_{r' \in \mathbb{B}_j} F_{r'j}^{lk} P_j^{r'}} = a_k^r \gamma$$

It means that if D2D pair k is active in RB r, then on all subcarrier l of RB r, the target SINR γ will be reached. This set of constraints is equivalent to KL equations, one per D2D pair and one per subcarrier:

$$P_k^r - a_k^r \gamma \sum_{j=0;j\neq k}^{K-1} \sum_{r' \in \mathbb{B}_j} F_{r'j}^{lk} P_j^{r'} = \frac{a_k^r \gamma n_k^l}{F_{rk}^{lk}}$$

In order to obtain a feasible solution to these equations, the variable vector $\boldsymbol{p}$ must be of the same size as the number of equations. However, because of the constraint of power allocation per RB, vector $\boldsymbol{p}$ is of size KR. In order to solve this problem, we introduce a temporary power vector per subcarrier $\tilde{p}$ and then impose the same power per RB constraint once the resource allocation algorithm is finished.
Similarly, the allocation variable is set per subcarrier $\tilde{a}$ such that $\tilde{a}(l + kL) = \tilde{a}_k^l$, but with the following constraint: $\tilde{a}_k^l = a_k^r$, for any $l \in \mathbb{R}_r$
By temporarily removing constraint (4), matrix $\boldsymbol{F}$ is replaced by $\tilde{G}$, and the KL equations can be written with matrix notations as follows:

$$\left(I_{KL} - \Gamma \widetilde{G_{dir}^{-1}} \widetilde{G_{int}}\right)\tilde{p} = \widetilde{G_{dir}^{-1}} \Gamma n$$

where:

- $\widetilde{G_{dir}}$ is the KL*KL diagonal matrix extracted from $\tilde{G}$ by only taking its diagonal values. It thus corresponds to all direct channel gains.
- $\widetilde{G_{int}} = \tilde{G} - \widetilde{G_{dir}}$ is the KL*KL matrix of interfering channel gains.
- Γ is a diagonal KL*KL matrix such that $\Gamma(l + kL, l + kL) = \tilde{a}_k^l \gamma$
- n is the KL*1 noise vector with $n(l + kL) = n_k^l$

To simplify notations, in the following, we note $\psi = \Gamma \widetilde{G_{dir}^{-1}} \widetilde{G_{int}}$.

Let ρ(ψ) be the spectral radius of matrix ψ. It is equal to the largest modulus of the eigenvalues of ψ. By Perron-Frobenius theorem, matrix $(I_{KL} - \psi)$ is invertible if matrix ψ has a spectral radius lower strictly lower than 1. Then a feasible positive power allocation leading to $\tilde{a}_k^l \gamma$ for all users and subcarriers (k,l) exists [16].

Consequently, the RB allocation algorithm proceeds as follows: it aims at determining the largest set of active D2D pairs in the RB, subject to the constraint that when the selected D2D pairs are active in the selected RBs, the power allocation allowing to reach the target SINR on all subcarriers of all active RBs should be feasible. This is equivalent to finding the largest set of active D2D pairs in the RB, such that the spectral radius of matrix ψ is strictly less than 1. The RB allocation problem is consequently written as follows:

$$argmax_{\tilde{a}\in\{0,1\}^{K*L}} \sum_{k=0}^{K-1}\sum_{l=0}^{L-1} \bar{a}_k^l$$
$$s.t.\ \rho(\psi) < 1$$
$$s.t.\ \tilde{a}_k^l = a_k^r, \forall\, l \in \mathbb{R}_r, \forall k \in \{0,\dots,K-1\}$$

This problem is highly complex since there are 2^{KN} combinations in vector $\boldsymbol{a}$ and for each combination, computing the spectral radius of ψ requires $O(KL^3)$ operations.
In order to override these limitations, we propose a heuristic of lower complexity based on the infinity norm. It is based on the following property of the spectral radius: the spectral radius is upper-bounded by any norm of matrix ψ.

4.2 Heuristic based on the infinity norm

Since $\rho(\psi) \leq \|\psi\|_\infty$, the constraint $\|\psi\|_\infty < 1$ implies that the spectral radius of matrix ψ is strictly less than 1. This constraint is more restrictive than the original one and will therefore provide a lower bound on the solution of the original problem, that is, the achieved multiplexing gain will be lower. However, using the infinity norm $\|\rho(\psi)\|_\infty < 1$ provides a criteria that is distributed and requires a low computational complexity.

The optimization problem with the infinity norm is:

$$argmax_{\tilde{a}\in\{0,1\}^{K*L}} \sum_{k=0}^{K-1}\sum_{l=0}^{L-1} \bar{a}_k^l$$
$$s.t.\ \|\psi\|_\infty < 1$$
$$s.t.\ \tilde{a}_k^l = a_k^r, \forall\, l \in \mathbb{R}_r, \forall k \in \{0,\dots,K-1\}$$

The infinity norm $\|\psi\|_\infty$ is written as follows:

$$\|\psi\|_\infty = max_{0\leq k\leq K-1, 0\leq l\leq L-1} \sum_{j=0}^{K-1}\sum_{l'=0}^{L-1} (\psi)(l+kL, l'+jL)$$

By definition of matrix ψ, it is equal to:

$$\|\psi\|_\infty = max_{0\leq k\leq K-1, 0\leq l\leq L-1}\, \tilde{a}_k^l \gamma \sum_{j=0}^{K-1}\sum_{l'=0}^{L-1} \frac{\tilde{G}(l+kL, l'+jL)}{\tilde{G}(l+kL, l+kL)}$$

To simplify notations, let us define E_k^l:

$$E_k^l = \gamma \sum_{j=0}^{K-1}\sum_{l'=0}^{L-1} \frac{\tilde{G}(l+kL, l'+jL)}{\tilde{G}(l+kL, l+kL)}$$

Constraint $\|\psi\|_\infty < 1$ is then equivalent to $\bar{a}_k^l E_k^l < 1$ for all (k,l). This constraint is only fulfilled if $\bar{a}_k^l = 0$ whenever $E_k^l \geq 1$. This solution is optimal since all values of $\bar{a}_k^l$ are equal to 1, except those that would violate condition $\|\psi\|_\infty < 1$. The sum of $\bar{a}_k^l$ under this constraint is then at its maximum. Finally, since resource allocation is performed per RB, if $E_k^l \geq 1$ on at least one subcarrier $l \in \mathbb{R}_r$, then D2D pair k is not multiplexed on RB r.

The infinity norm provides a distributed algorithm: at each receiver, E_k^l is computed depending on local information, that is deduced from the received interfering channel gains. This feature is quite appealing for future implementation of this algorithm in practical D2D networks.

This algorithm can be either combined with the power allocation algorithm from Section 3 if the D2D transmissions happen in an underlay context, or the power values can be directly obtained by inverting matrix $\left(I_{KL} - \Gamma \widetilde{G_{dir}^{-1}} \widetilde{G_{int}}\right)$ as follows:

$$\tilde{p} = \left(I_{KL} - \Gamma \widetilde{G_{dir}^{-1}} \widetilde{G_{int}}\right)^{-1} \widetilde{G_{dir}^{-1}} \Gamma n$$

Since this power vector is defined per subcarrier, the transmit power of transmitter k in RB r is finally chosen as the maximum transmit power of k in all subcarriers of RB r.
It should be noticed that these power values do not take into account any interference level constraint at the BS and should consequently only be used when devices are not operating in underlay mode. In this case, they provide power values allowing to achieve a SINR at least equal to γ on all the subcarriers of the RB that are allocated to each user.
In the following, we provide simulation results relative to this scenario, because or objective is to evaluate the highest multiplexing gain.

4.3 Simulation results

The simulation assumptions are the same as in section 2.2, except that there is no Base Station and only K D2D pairs are considered.
The performances of maximum multiplexing heuristics are compared with a Frequency Division Multiple Access (FDMA) solution, where each D2D pairs gets the same amount of RB, and RB are randomly allocated to D2D pairs. Each D2D transmitter then uses equal power allocation on its allocated RB.

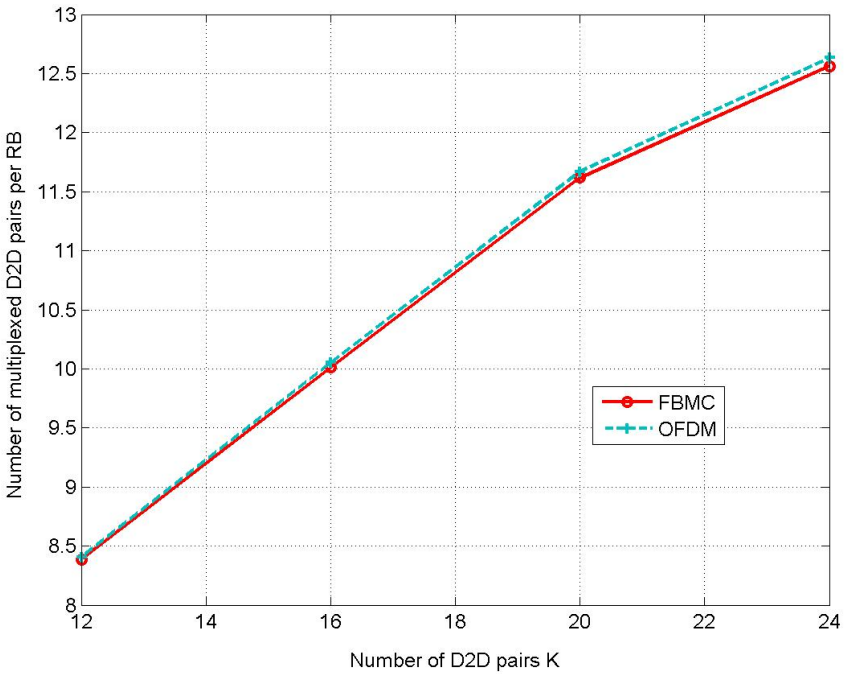

Figure 3: Average number of multiplexed D2D pairs

Figure 3 shows that the average data rate is greatly improved by multiplexing. In FDMA, the number of D2D pairs per RB would be one ; with the proposed algorithm, more than half of the D2D pairs are active in each RB.

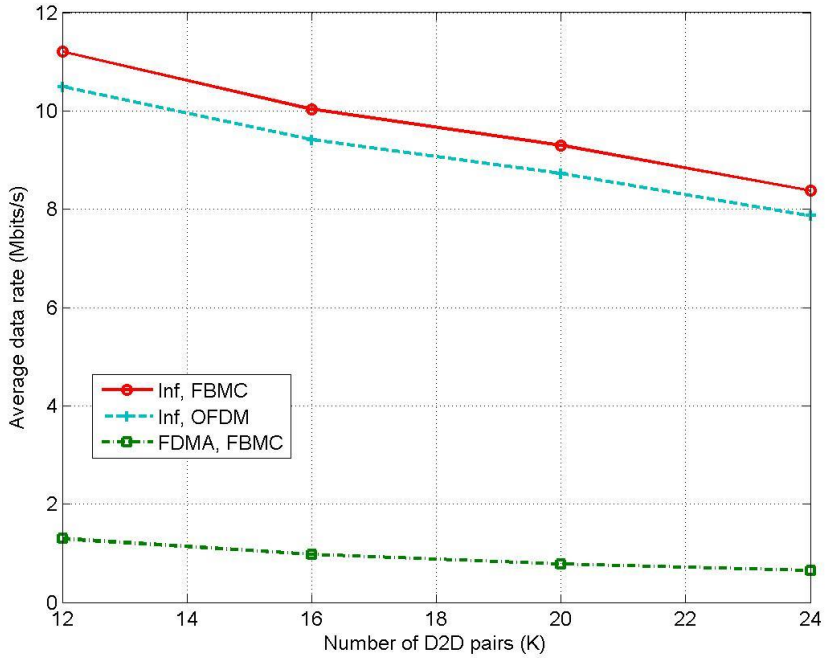

Figure 4: Average data rate depending on the multiplexing technique

Moreover, Figure 4 shows that the average data rate achieved with our proposed algorithm is higher with FBMC-OQAM than with OFDM because there is no overhead due to cyclic prefix. Since power values and interferences are very low, the influence of ICI is almost negligible in this scenario, contrary to what was obtained with larger rates and power control in Section 3.

To conclude, the proposed algorithm based on the infinity criterion allows to multiplex a very large number of D2D pairs and to achieve high data rates. This algorithm is of low complexity and can be implemented in a distributed way.

5 COW-CFMC: a new waveform for asynchronous multi-user access

In this section, we propose a new scheme that preserves the advantages of WCP-COQAM [1] while guaranteeing in the complex orthogonality. Indeed, WCP-COQAM is based on block processing and uses circular filtering in order to remove time overheads. However, like FBMC/OQAM scheme, WCP-COQAM suffers from the presence of intrinsic interference that prevents some MIMO techniques such as Alamouti Coding. This intrinsic interference results from the non-complex orthogonal property of WCP-COQAM and FBMC/OQAM. In the following, we show that circular filtering makes the transmultiplexer impulse response circulant. Our proposed scheme, called COW-CFMC presented in [2], exploits this circularity to restore the complex orthogonality by precoding the data symbols in each subcarrier.

5.1 Review and properties of WCP-COQAM

A new concept of multi-carrier modulation has recently appeared in the literature where the linear filtering is replaced by a circular filtering for pulse shaping [1][3]. A periodic filter is used to realize the circular convolution at the transmitter, which is equivalent to the tail-biting process. This idea was originally proposed with the introduction of Generalized Frequency Division Multiplexing (GFDM) [4]. Thanks to the use of a circular filtering, the overall multicarrier modulation system can be seen as a block transform processing and a Cyclic Prefix (CP) is inserted to enhance the orthogonality under multi-path channel. In [1], the authors have also adopted the circular filtering to FBMC. In order to cope with the multi-path interference and to prevent the degradation of the PSD due to the block processing, a CP and a windowing are added. This scheme is called Windowed Cyclic Prefix FBMC/circular OQAM (WCP-COQAM).

5.1.1 Review on WCP-COQAM

First of all, we recall the baseband discrete time model of the classical FBMC/OQAM. The transmitted signal $s[m]$ in FBMC/OQAM can be written as follows [5]:

$$s[m] = \sum_{k=0}^{M-1} \sum_{n \in Z} a_{k,n} g[m - nM/2] e^{j\frac{2\pi k}{M}(m-D)} e^{j\phi_{k,n}}, \quad (1)$$

where M is the number of subcarriers, $a_{k,n}$ are the real-valued transmitted symbols at time index n and subcarrier k, D is the delay term to insure the causality. This delay depends on the length L_g of the prototype filter response $g[m]$, $L_g = KM$ where K is the overlapping factor. The phase term $\phi_{k,n}$ is given by [5]:

$$\phi_{k,n} = \frac{\pi}{2}(n+k) - \pi kn \quad (2)$$

In [1], the authors have proposed to replace the linear convolution used in FBMC/OQAM with a circular convolution similar to the GFDM and CB-FMT. The main advantage of the so-called circular OQAM (COQAM) scheme is removing the time overheads caused by the linear filtering and the OQAM structure itself.

Circular filtering implies block-wise processing. Assuming that N is the number of real symbol slots per block and M is the subcarrier number, the transmitted signal block has a length of $MN/2$. The discrete-time COQAM signal $s[m]$, with $m \in \{0, \dots, MN/2 - 1\}$, is expressed as [1]:

$$s[m] = \sum_{k=0}^{M-1} \sum_{n=0}^{N-1} a_{k,n} \tilde{g}[m - nM/2] e^{j\frac{2\pi k}{M}(m-D)} e^{j\phi_{k,n}}, \quad (3)$$

where the prototype filter response $\tilde{g}[m]$ is obtained by performing the periodic repetition of the initial prototype filter $g[m]$ as follows:

$$\tilde{g}[m] = g\left[|m|_{\frac{MN}{2}}\right] \quad (4)$$

where $|m|_N$ stands for the modulo operation by N. It is worth noting that the authors in [1] set the overlapping factor $K = N/2$. That is, the initial prototype filter $g[m]$ has the same length $L_g = KM = MN/2$ as the transmitted signal block.

In order to keep the orthogonality after the transmission over a frequency selective channel, a cyclic prefix (CP) is added to the transmitted signal block $s[m]$, $m \in \{0, \dots, MN/2 - 1\}$. Furthermore, due to the degradation of the PSD resulting from the block processing, a windowing before the transmission also has to be applied. The overall scheme is called WCP-COQAM [1]. The CP of length L_{CP} is composed of two parts : the guard interval of length L_{GI} to fight the interference due to multi-path channel effect and the part dedicated to the windowing transitions L_{RI}.

At the received side, the overall CP is first removed and then the demodulated received symbols $y_{q,l}$ in subcarrier $q \in \{0, \dots, M-1\}$ and time index $l \in \{0, \dots, N-1\}$ can be obtained as follows:

$$y_{q,l} = \sum_{m=0}^{MN/2-1} s[m] \tilde{g}[m - lM/2] e^{-j\frac{2\pi q}{M}(m-D)} e^{-j\phi_{q,l}} \quad (5)$$

5.1.2 Properties of Circular OQAM

In this subsection, we will demonstrate that the transmultiplexer impulse response in WCP-COQAM is circulant. By plugging the expression of $s[m]$ given by (3) into (5) we obtain the expression of the demodulated received symbols $y_{q,l}$ written as:

$$y_{q,l} = \sum_{k=0}^{M-1} \sum_{n=0}^{N-1} a_{k,n} \sum_{m=0}^{MN/2-1} \tilde{g}[m - nM/2] \tilde{g}[m - lM/2] \times e^{j\frac{2\pi(k-q)}{M}(m-D)} e^{j\phi_{k,n} - j\phi_{q,l}} \quad (6)$$

Let us define $\Gamma_{q,k}(l,n)$ as:

$$\Gamma_{q,k}(l,n) = \sum_{m=0}^{MN/2-1} \tilde{g}[m - nM/2] \tilde{g}[m - lM/2] \times e^{j\frac{2\pi(k-q)}{M}(m-D)} e^{j\phi_{k,n} - j\phi_{q,l}} \quad (7)$$

Therefore, according to (6) and (7), we can write:

$$y_{q,l} = \sum_{k=0}^{M-1} \sum_{n=0}^{N-1} \Gamma_{q,k}(l,n) a_{k,n} \quad (8)$$

The function $\Gamma_{q,k}(l,n)$ given in (7) is proportional to the $M/2$-downsampled correlation function between the frequency shifted versions of $\tilde{g}[m]$, shifted by $\frac{2\pi km}{M}$ and $\frac{2\pi qm}{M}$. In the other hand, the prototype filter $g[m]$ is assumed to be frequency well localized such that the spectrum of the signal in a given subcarrier is only spread over both immediate adjacent subcarriers [6]. Therefore, the function $\Gamma_{q,k}(l,n)$ is negligible if $|q-k| > 1$. Hence, the summation in (8) with respect to k can be simplified to be only over the set $\{q-1, q, q+1\}$.

In a matrix form, the vector $\mathbf{y}_q = [y_{q,0}, \dots, y_{q,N-1}]^T$ of size $N \times 1$ containing the N demodulated symbols in a given subcarrier q can be hence expressed as:

$$\mathbf{y}_q = \sum_{k=q-1}^{q+1} \mathbf{\Gamma}_{q,k}\mathbf{a}_k \tag{9}$$

where $\mathbf{\Gamma}_{q,k}$ is a $N \times N$ matrix whose entries are $\Gamma_{q,k}(l,n)$ in the l-th row and n-th column, and $\mathbf{a}_k = [a_{k,0},\dots,a_{k,N-1}]^T$ is the vector of size $N \times 1$ containing the N transmitted symbols in subcarrier k.

In the following, we shall demonstrate that the matrix $\mathbf{\Gamma}_{q,k}$ is circulant $\forall(q,k) \in \{0,\dots,M-1\}^2$. To begin with, we substitute $m - lM/2$ by m in (7). Hence, we obtain:

$$\Gamma_{q,k}(l,n) = \sum_{m=-l\frac{M}{2}}^{MN/2-lM/2-1} \tilde{g}[m]\tilde{g}[m-(n-l)M/2] \times e^{j\frac{2\pi(k-q)}{M}(m-D)} e^{j\pi l(k-q)} e^{j\phi_{k,n}-j\phi_{q,l}} \tag{10}$$

After that, since $l \geq 0$, we can split the sum over m as

$$\Gamma_{q,k}(l,n) = \sum_{m=-l\frac{M}{2}}^{-1} \tilde{g}[m]\tilde{g}[m-(n-l)M/2] e^{j\frac{2\pi(k-q)}{M}(m-D)} e^{j\frac{\pi}{2}(k-q+n-l)} e^{j\pi(l-n)k} + \sum_{m=0}^{MN/2-lM/2-1} \tilde{g}[m]\tilde{g}[m-(n-l)M/2] e^{j\frac{2\pi(k-q)}{M}(m-D)} e^{j\frac{\pi}{2}(k-q+n-l)} e^{j\pi(l-n)k} \tag{11}$$

where the phase terms ϕ are replaced by their terms given by (2). According to the definition of $\tilde{g}[m]$ given by (4) and the fact that $l \in \{0,\dots,N-1\}$, we have:

$$\begin{cases} \tilde{g}[m] = g\left[m + \frac{MN}{2}\right] & \text{if } m \in \left\{-l\frac{M}{2},\dots,-1\right\} \\ \tilde{g}[m] = g[m] & \text{if } m \in \left\{0,\dots,\frac{MN}{2} - l\frac{M}{2} - 1\right\} \end{cases} \tag{12}$$

Therefore, we can rewrite (11) as:

$$\Gamma_{q,k}(l,n) = \sum_{m=-l\frac{M}{2}}^{-1} g[m+MN/2]\tilde{g}[m-(n-l)M/2] e^{j\frac{2\pi(k-q)}{M}(m-D)} e^{j\frac{\pi}{2}(k-q+n-l)} e^{j\pi(l-n)k} + \sum_{m=0}^{MN/2-lM/2-1} g[m]\tilde{g}[m-(n-l)M/2] e^{j\frac{2\pi(k-q)}{M}(m-D)} e^{j\frac{\pi}{2}(k-q+n-l)} e^{j\pi(l-n)k} \tag{13}$$

Subtituting $m + MN/2$ by m in the first summation term, we obtain:

$$\Gamma_{q,k}(l,n) = \sum_{m=\frac{MN}{2}-l\frac{M}{2}}^{\frac{MN}{2}-1} g[m]\tilde{g}\left[m-(n-l)\frac{M}{2}-\frac{MN}{2}\right] e^{j\frac{2\pi(k-q)}{M}(m-D)} e^{j\frac{\pi}{2}(k-q+n-l)} e^{j\pi(l-n)k} + \sum_{m=0}^{MN/2-lM/2-1} g[m]\tilde{g}[m-(n-l)M/2] e^{j\frac{2\pi(k-q)}{M}(m-D)} e^{j\frac{\pi}{2}(k-q+n-l)} e^{j\pi(l-n)k} \tag{14}$$

According to the periodicity of $\tilde{g}[m]$ (that is $\tilde{g}[m-MN/2] = \tilde{g}[m]$), we can recombine both summation terms in the equation above and write:

$$\Gamma_{q,k}(l,n) = \sum_{m=0}^{\frac{MN}{2}-1} g[m]\tilde{g}[m-(n-l)M/2] e^{j\frac{2\pi(k-q)}{M}(m-D)} e^{j\frac{\pi}{2}(k-q+n-l)} e^{j\pi(l-n)k} \tag{15}$$

To prove that the matrices $\mathbf{\Gamma}_{q,k}$ ($\forall(q,k) \in \{0,\dots,M-1\}^2$) are circulant, we can proceed by demonstrating that:

$$\forall(q,k) \in \{0,\dots,M-1\}^2, \forall(l,n) \in \{0,\dots,N-1\}^2, \forall\delta \in \mathbb{Z}:$$
$$\Gamma_{q,k}(|l+\delta|_N, |n+\delta|_N) = \Gamma_{q,k}(l,n) \tag{16}$$

First of all, we recall some properties about modulo operation: $\forall(l,n,N,M) \in \mathbb{Z}^4$, we have

$$|n+l|_N = ||n|_N + |l|_N|_N \tag{17}$$

$$|Mn|_{MN} = M|n|_N \tag{18}$$

Therefore, according to (4), we can rewrite the term $\tilde{g}[m-(n-l)M/2]$ in (15) as

$$\begin{aligned}\tilde{g}\left[m-(n-l)\frac{M}{2}\right] &= g\left[\left|m-(n-l)\frac{M}{2}\right|_{\frac{MN}{2}}\right]\\ &= g\left[\left|m-\left|(n-l)\frac{M}{2}\right|_{\frac{MN}{2}}\right|_{\frac{MN}{2}}\right]\\ &= g\left[\left|m-\frac{M}{2}|n-l|_N\right|_{\frac{MN}{2}}\right]\\ &= \tilde{g}\left[m-\frac{M}{2}|n-l|_N\right]\end{aligned} \tag{19}$$

where the second equality holds because $|m|_{\frac{MN}{2}} = m$ since in (15) the summation on m is over $\{0,\dots,MN/2-1\}$. In the other hand, we can calculate $\Gamma_{q,k}(|l+\delta|_N, |n+\delta|_N)$ as

$$\begin{aligned}&\Gamma_{q,k}(|l+\delta|_N, |n+\delta|_N)\\ &= \sum_{m=0}^{\frac{MN}{2}-1} g[m]\tilde{g}\left[m-(|n+\delta|_N-|l+\delta|_N)\frac{M}{2}\right]e^{j\frac{2\pi(k-q)}{M}(m-D)}e^{j\frac{\pi}{2}(k-q)}\Phi_k(|l+\delta|_N, |n+\delta|_N)\end{aligned} \tag{20}$$

where $\Phi_k(l,n) = e^{j\frac{\pi}{2}(n-l)}e^{j\pi(l-n)k}$. Using the definition of $\tilde{g}[m]$ given in (4) and taking into account the properties given in (17)-(18), we have

$$\tilde{g}\left[m-(|n+\delta|_N-|l+\delta|_N)\frac{M}{2}\right]$$

$$= g\left[\left|m-(|n+\delta|_N-|l+\delta|_N)\frac{M}{2}\right|_{\frac{MN}{2}}\right] \tag{21}$$

$$= g\left[\left|m-\left|(|n+\delta|_N-|l+\delta|_N)\frac{M}{2}\right|_{\frac{MN}{2}}\right|_{\frac{MN}{2}}\right] \tag{22}$$

$$= g\left[\left|m-\frac{M}{2}||n+\delta|_N-|l+\delta|_N|_N\right|_{\frac{MN}{2}}\right] \tag{23}$$

$$= g\left[\left|m-\frac{M}{2}|n-l|_N\right|_{\frac{MN}{2}}\right] \tag{24}$$

$$= \tilde{g}\left[m-\frac{M}{2}|n-l|_N\right] \tag{25}$$

Hence, from equations (19) and (25), we can deduce that for $m \in \{0,\dots,MN/2-1\}$ we have:

$$\tilde{g}\left[m-(|n+\delta|_N-|l+\delta|_N)\frac{M}{2}\right] = \tilde{g}\left[m-(n-l)\frac{M}{2}\right] \tag{26}$$

Moreover, we can develope the phase term $\Phi_k(.,.)$ in (20) as:

$$\Phi_k(|l+\delta|_N, |n+\delta|_N) = e^{j\frac{\pi}{2}(|n+\delta|_N-|l+\delta|_N)}e^{j\pi k(|l+\delta|_N-|n+\delta|_N)} \tag{27}$$

We can easily show that:

$$\forall (p,c) \in \mathbb{Z}_*^2,: \quad e^{j\frac{2\pi}{c}n} = e^{j\frac{2\pi}{c}|n|_{pc}} \tag{28}$$

Therefore, assuming that N is multiple of 4, we can deduce that:

$$\Phi_k(|l+\delta|_N, |n+\delta|_N) = e^{j\frac{\pi}{2}(n-l)}e^{j\pi k(l-n)} \tag{29}$$

Finally, according to (29) and (26), we rewrite (20) as

$$\Gamma_{q,k}(|l+\delta|_N, |n+\delta|_N) = \sum_{m=0}^{\frac{MN}{2}-1} g[m]\tilde{g}\left[m-(n-l)\frac{M}{2}\right]e^{j\frac{2\pi(k-q)}{M}(m-D)}e^{j\frac{\pi}{2}(k-q+n-l)}e^{j\pi k(l-n)} \tag{30}$$

which is the same expression as that of $\Gamma_{q,k}(l,n)$ given in (15). This shows that condition (16) is satisfied, which proves that the matrices $\mathbf{\Gamma}_{q,k}$, $(q,k) \in \{0,\dots,M-1\}^2$ are circulant.

Therefore, the matrices $\mathbf{\Gamma}_{q,k}$ are diagonalizable by the discrete Fourier transform (DFT) matrix $\mathbf{W}$ and their eigenvalues are the DFT coefficients of the sequences $\{\Gamma_{q,k}(l,0), l \in \{0,\dots,N-1\}\}$. Hence, we can rewrite (9) as:

$$\mathbf{y}_q = \sum_{k=q-1}^{q+1} \mathbf{W}^H \mathbf{D}_{q,k} \mathbf{W} \mathbf{a}_k \quad (31)$$

where $\mathbf{D}_{q,k}$ is the diagonal matrix obtained by diagonalizing $\mathbf{\Gamma}_{q,k}$ by the unitary matrix $\mathbf{W}$. Therefore, the diagonal elements in $\mathbf{D}_{q,k}$ are given by:

$$\mathbf{D}_{q,k}(l,l) = \sum_{l'=0}^{N-1} \Gamma_{q,k}(l',0) e^{-j\frac{2\pi}{N}ll'} \quad (32)$$

where, according to (15),

$$\Gamma_{q,k}(l',0) = \sum_{m=0}^{\frac{MN}{2}-1} g[m]\tilde{g}[m+l'M/2] e^{j\frac{2\pi(k-q)}{M}(m-D)} e^{j\frac{\pi}{2}(k-q-l')} e^{j\pi l'k}$$

5.2 COW-CFMC description

For both FBMC and WCP-COQAM, the presence of the intrinsic interference prevents the combination with some MIMO techniques such as space-time block coding and spatial multiplexing (SM) with maximum likelihood (ML) detection [6][7]. Another FBMC scheme (named FFT-FBMC) was proposed in [8]. This scheme performs IFFT precoding and FFT decoding with CP insertion on each subcarrier in order to suppress the FBMC intrinsic interference. It was shown that MIMO techniques such as Space-Time Block Coding (STBC) and SM-ML can be performed straightforwardly in FFT-FBMC [9]. However, like the FBMC scheme, FFT-FBMC still suffers from the time overhead when short data bursts are considered due to the signal ramp-up/ramp-down and the half symbol offset overhead.

Hence, we propose a new scheme that combine the advantages of both WCP-COQAM and FFT-FBMC. That is, we aim to remove the edge time transitions as well as the half symbol offset overhead while guartaneeing the complex orthogonality. Indeed, we propose to replace the classical linear filtering by a circular one in the previously proposed FFT-FBMC schme. Or alternatively, it can also be seen as proposing to introduce IFFT precoding and FFT decoding in each subcarrier to the WCP-COQAM scheme. We call our proposed scheme Complex Orthogonal Windowed CP Circular Filtered Multi-Carrier (COW-CFMC). As we have aforementioned, a CP insertion in each subcarrier was proposed for FFT-FBMC to make the transmultiplexer impulse response circulant. However, we will show that thanks to the use of circular filtering, the transmultiplexer impulse response is already circulant in WCP-COQAM. Therefore, for our proposed COW-CFMC scheme, there is no need to insert a CP in each subcarrier. Thus, the proposed system has a good spectral efficiency and and guarantees the complex orthogonality. Thanks to this last property, the scheme can be easily coupled with MIMO techniques such as STBC and SM-ML.

Equation (31) shows that WCP-COQAM does not guarantee the complex orthogonality and then the received demodulated symbols are affected by the intrinsic interference. This interference is also present in the classical FBMC/OQAM. In order to enable the complex orthogonality for FBMC, the authors in [9] proposed to precode the data symbols in each subcarrier by performing a IDFT. Before being fed to the FBMC modulator, the IDFT outputs are appended with a CP to make the transmultiplexer impulse response circulant. At the receiver side, the CPs are removed after the FBMC demodulator, and then the DFT is performed in each subcarrier to recover the data symbols. It is worth noticing that a special transmission strategy is still required to guarantee the complex orthogonality. In the following, we apply the same principle above to the WCP-COQAM scheme and explain the processing in more details.

Therefore, similarly as in [9], let us consider that the transmitted symbol block $\mathbf{a}_k$ in subcarrier k is the IDFT output of a data symbol block $\mathbf{d}_k$ (*i.e.* $\mathbf{a}_k = \mathbf{W}^H \mathbf{d}_k$). Hence, taking the DFT of the received block $\mathbf{y}_q$ in subcarrier q, we obtain from (31) the following:

$$\begin{aligned} \mathbf{r}_q &= \mathbf{W}^H \mathbf{y}_q = \sum_{k=q-1}^{q+1} \mathbf{D}_{q,k} \mathbf{W} \mathbf{a}_k \\ &= \mathbf{D}_{q,q}\mathbf{d}_q + \mathbf{D}_{q,q-1}\mathbf{d}_{q-1} + \mathbf{D}_{q,q+1}\mathbf{d}_{q+1} \end{aligned} \quad (34)$$

The two last terms represent the interference coming from the immediate adjacent subcarriers $q \pm 1$.

According to (32), the coefficients in the diagonal matrix $\mathbf{D}_{q,q}$ are the N-DFT of $\Gamma_{q,q}(l',0)$ which is, according to (33), given by:

$$\Gamma_{q,q}(l',0) = \underbrace{\sum_{m=0}^{\frac{MN}{2}-1} g[m]\tilde{g}[m+l'M/2]}_{R_{\tilde{g}}[l'\frac{M}{2}]} e^{-j\frac{\pi}{2}l'} e^{j\pi l'q} \quad (35)$$

We note that $R_{\tilde{g}}[l'\frac{M}{2}]$ is the $\frac{M}{2}$-downsampled autocorrelation function of the periodic filter $\tilde{g}[m]$ (please also note that $g[m] = \tilde{g}[m]$ for $0 \leq m < MN/2$). Since we consider, as we have previously mentionned, that the filter $g[m]$ is at least spectrally confined in $[-\frac{1}{M}, \frac{1}{M}]$, downsampling the autocorrelation function $R_{\tilde{g}}[l']$ by $M/2$ does not cause aliasing and

hence the spectrum shape of $R_{\tilde{g}}[l']$ is preserved. Fig. 5 illustrates an example, using Mirabbasi-Martin [10] filter with $K = 8$, of the spectrum $G[l]$ of $R_{\tilde{g}}[l'\frac{M}{2}]$ obtained by $G[l] = \sum_{l'=0}^{N-1} R_{\tilde{g}}[l'\frac{M}{2}]e^{-j\frac{2\pi}{N}ll'}$.

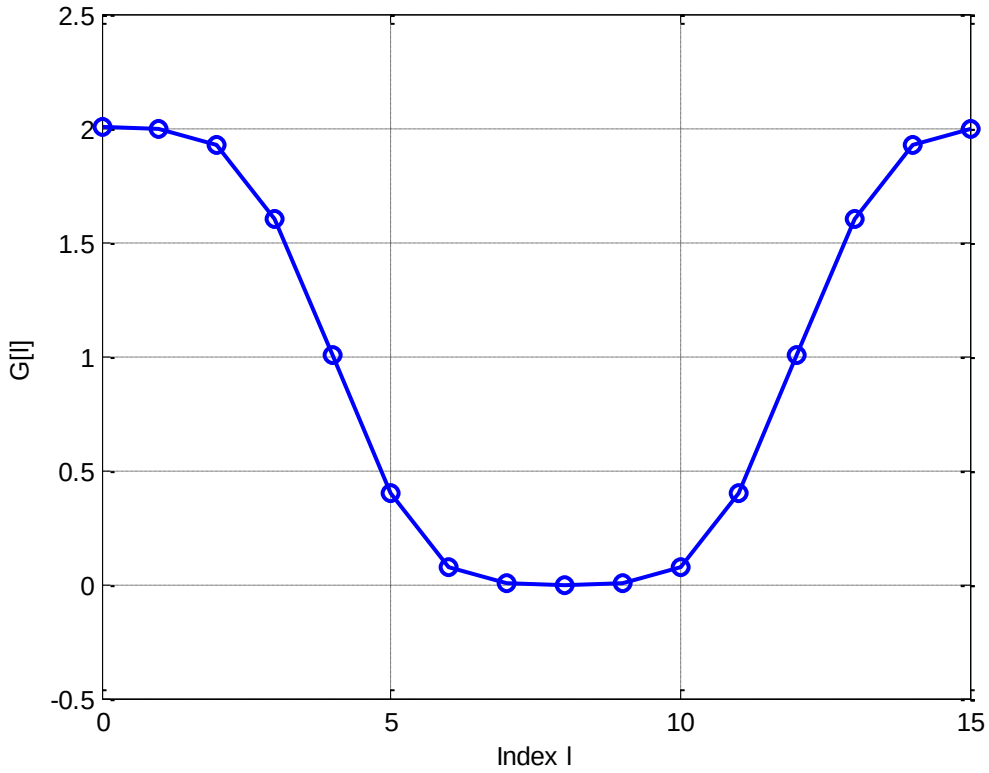

Figure 5: Spectrum of the M/2-downsampled autocorrelation function of the periodic Mirabbasi-Martin filter $\tilde{g}[m]$ with overlapping factor K=8.

Therefore, equation (35) shows that $\Gamma_{q,q}(l',0)$ is the phase-shifted by $e^{-\frac{\pi}{2}l'}e^{j\pi ql'}$ version of $R_{\tilde{g}}[l'\frac{M}{2}]$. Thus, according to (32), the coefficients $\mathbf{D}_{q,k}(l,l)$ are the circularly shifted version of $G[l]$ by $\frac{N}{2}q - \frac{N}{4}$ to the right. Hence, we can write:

$$\mathbf{D}_{q,q}(l,l) = G\left[\left|l - \frac{N}{2}q + \frac{N}{4}\right|_N\right] \quad (36)$$

Therefore, the coefficients in the diagonal matrix $\mathbf{D}_{q,q}(l,l)$ depend on the parity of q. Fig. 2 illustrates the coefficients $\mathbf{D}_{q,q}(l,l)$ for q even and odd.

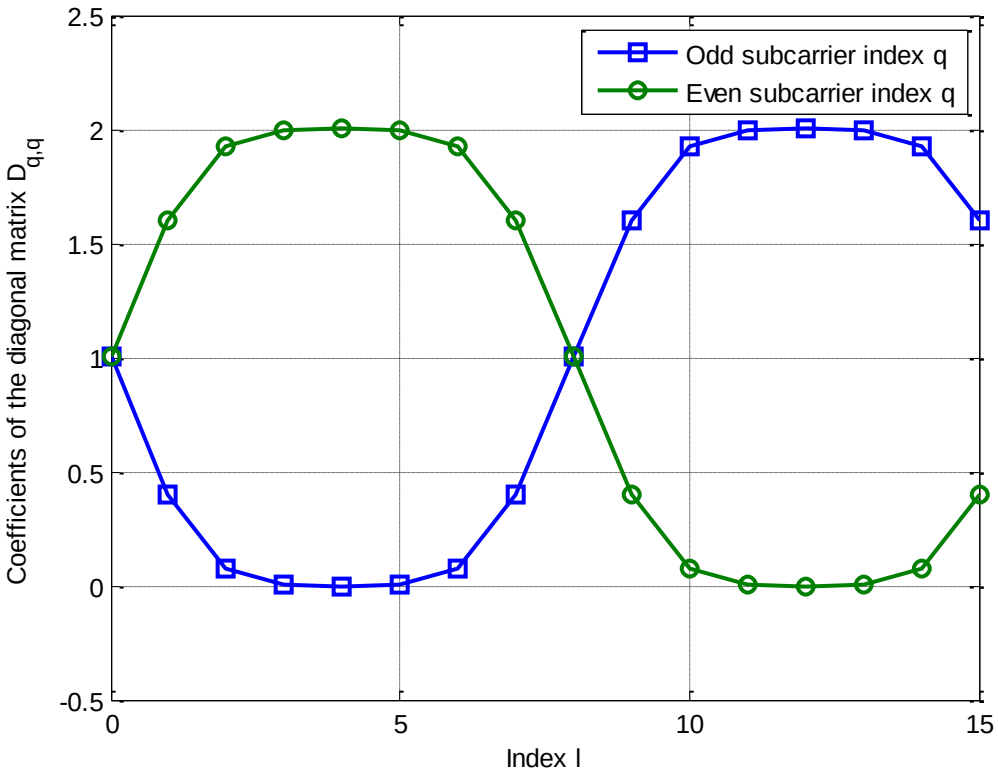

Figure 6: Coefficients of the diagonal matrix D_(q,q) for even and odd subcarrier index q using Mirabbasi-Martin filter with overlapping factor K=8.

In order to avoid interference terms in (34), we propose, as in [8][9], to only transmit useful complex data symbols in the first half N-block when the subcarrier index q is even, and in the second half N-block when the subcarrier index q is odd (please see Fig. 6). That is, we can write:

$$\mathbf{d}_q = \begin{cases} \left[\bar{\mathbf{d}}_q^T, \mathbf{0}^T\right]^T \text{ if q is even} \\ \left[\mathbf{0}^T, \bar{\mathbf{d}}_q^T\right]^T \text{ if q is odd} \end{cases} \tag{37}$$

where $\bar{\mathbf{d}}_q$ is a $(\frac{N}{2} \times 1)$-vector of complex data sumbols, and $\mathbf{0}$ is a zero vector of size $\frac{N}{2} \times 1$. Let us also set the following:

$$\mathbf{r}_q = \begin{bmatrix} \mathbf{r}_q^{(0)} \\ \mathbf{r}_q^{(1)} \end{bmatrix}, \text{and} \quad \mathbf{D}_{q,k} = \begin{bmatrix} \mathbf{D}_{q,k}^{(0)} & \bar{\mathbf{0}} \\ \bar{\mathbf{0}} & \mathbf{D}_{q,k}^{(1)} \end{bmatrix}, \tag{38}$$

where $\mathbf{r}_q^{(i)}$, $i \in \{0,1\}$ is a $(\frac{N}{2} \times 1)$-vector, and $\mathbf{D}_{q,k}^{(i)}$, $i \in \{0,1\}$ and $\bar{\mathbf{0}}$ are square matrices of size $\frac{N}{2} \times \frac{N}{2}$. Therefore, we can show that equation (34) becomes:

$$\mathbf{r}_q^{(i)} = \mathbf{D}_{q,q}^{(i)} \bar{\mathbf{d}}_q, \quad \text{for} \quad i = |q|_2 \tag{39}$$

This last expression shows that the transmitted complex data symbols $\bar{d}_{q,p} = \bar{\mathbf{d}}_q(p)$, $p \in \{0, \ldots, N/2 - 1\}$ are received free of interference because $\mathbf{D}_{q,q}^{(i)}$ is a diagonal matrix. Therefore, our proposed scheme satisfies the complex orthogonality and enables any transmission technique that requires complex orthogonality such as STBC and SM-ML. It is important to notice that compared to the FFT-FBMC, there is no need to add a cyclic prefix after the IFFT operation in each subcarrier thanks to the circular convolution.

5.3 Power spectrum density

In this section we will first evaluate the estimated power spectrum density (PDS) of the proposed COW-CFMC scheme with respect to other existing schemes. Following [1] for the evaluation, we have considered $M = 64$ with $M/2$ active subcarriers. We have compared the PSD of the proposed COW-CFMC scheme with the ones of the CP-OFDM, FFT-FBMC and WCP-COQAM schemes in Fig. 3. We have chosen $N = 16$ and $L_{GI} = L_{RI} = 16$ using Hamming window for the WCP-COQAM and COW-CFMC schemes. As for the prototype filter, we used the Mirabbasi-Martin

filter with overlapping factor $K = \frac{N}{2} = 8$. Fig. 7 shows that FFT-FBMC exhibits the best PSD. We can also observe that the proposed COW-CFMC scheme achieves the same PSD than the WCP-COQAM scheme. The relatively high PSD leakage of COW-CFMC and WCP-COQAM compared to the one of FFT-FBMC is due to the block processing. However, compared to CP-OFDM, COW-CFMC and WCP-COQAM schemes present lower spectrum leakage.

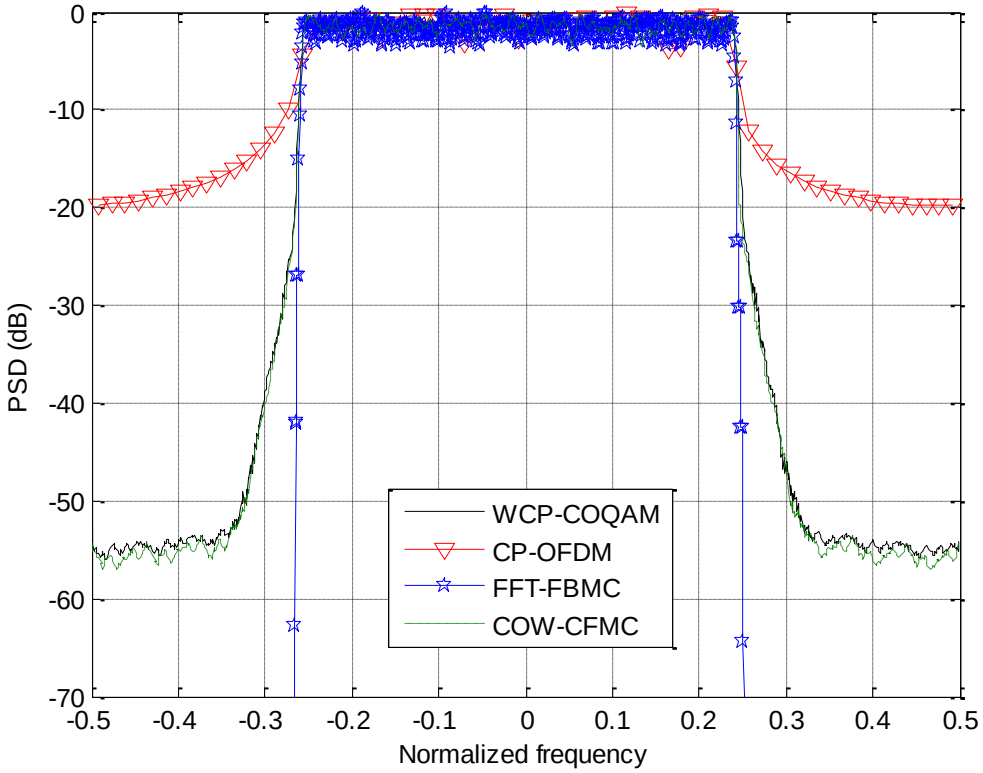

Figure 7: Power Spectrum Density evaluation of different schemes

In addition, we have also considered in Fig. 8 the case where 10 subcarriers are switched off using the same parameter settings as previously. The results show again that COW-CFMC and WCP-COQAM schemes have the same low radiation level in the empty band.

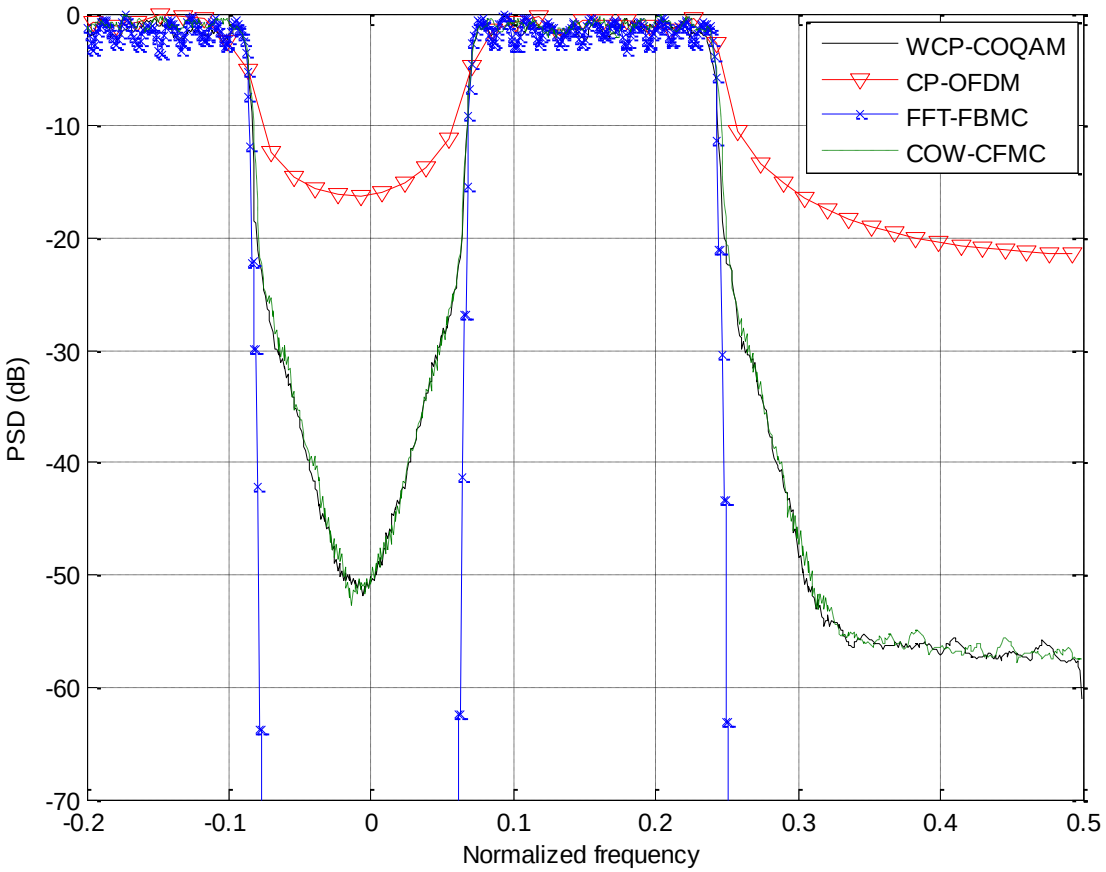

Figure 8: Power Spectrum Density evaluation of different schemes.

5.4 Robustness to time and frequency misalignment

In this section, we discuss the performance of the proposed waveform in multi-user asynchronous access. In order to focus on the asynchronous interference impact on the performance of the waveform, we propose to measure the normalized mean square error (NMSE) on decoding the useful symbols of the user of interest in ideal noiseless channel. Note that NMSE is adopted since it remains the same for all mapping constellations. Both per-subcarrier NMSE and average NMSE are assessed versus timing offset or carrier frequency offset (CFO). Actually, per-subcarrier NMSE can provide a meaningful information about the distribution of asynchronous interference across useful subcarriers. Several cases of guard-bands (between the interferer and the user of interest) are examined: $\delta = 0, 30, 120$ 195 kHz. Note that we use a color map indicating the NMSE levels: from dark blue color when the NMSE is less than or equal to −40dB to dark red color when the NMSE is greater than or equal to −10dB.
In this section we consider the COW-CFMC transceiver with $M = 64$ overlapped subbands and $N = 64$ subcarriers per subband which makes a total of $MN/2 = 2048$ available subcarriers. The subcarrier spacing is set to $\Delta f = 15$KHz.

5.4.1 Timing offset

In order to distinguish the degradation induced by timing synchronization errors from the one caused by the CFO, we consider in this subsection that there is no CFO ($\in= 0$ Hz) between the interfering signal and the useful one. The timing misalignment varies from -1024 to 1024 samples.

In Fig. 5, we can distinguish two regions: when the delay error is less than CP=32 samples, we observe in Fig. 9 a dark blue region (NMSE below -40 dB) which means that there is no asynchronous interference. Such a result is due to the fact that the orthogonality between subcarriers is maintained as long as the delay error does not exceed the CP duration. When the delay error exceeds the CP interval, the orthogonality is somewhat lost. This loss of orthogonality gives rise (but still acceptable) to a level of asynchronous interference. We can see that the interference level slowly decreases as

the spectral distance between the victim subcarrier and the interfering ones increases. Similarly, we observe a negligible enhancement when increasing the guard band.

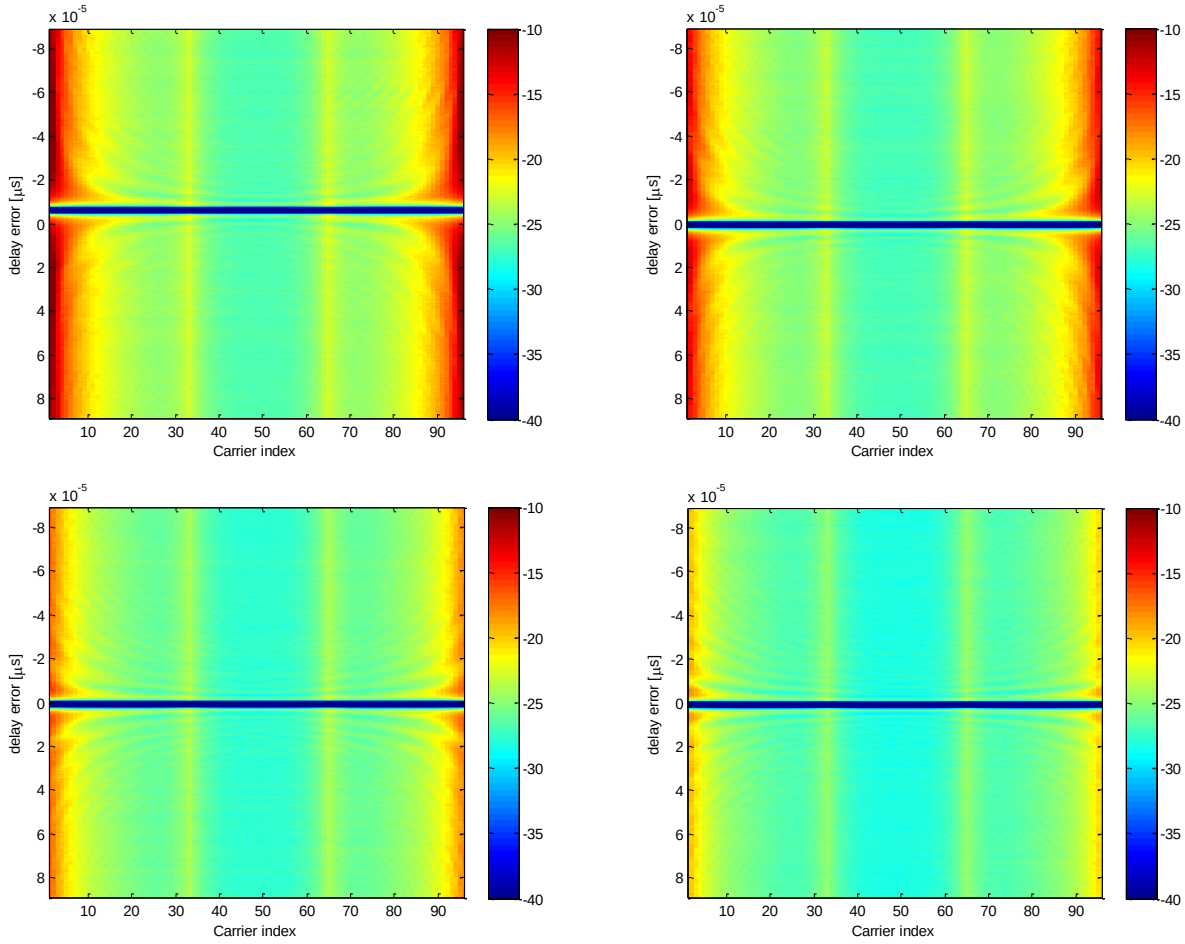

Figure 9: per-subcarrier NMSE against timing offset (samples).

The average NMSE of the waveform obtained over all subcarriers is plotted versus the timing offset in Fig. 10. In the CP region, we can observe that COW-CFMC achieves the pest performance with an NMSE lower than -50 dB. However, the best average NMSE outside of the CP region is about of -25 dB and is obtained when the band guard is 195 KHz. When there is no band guard between the interferer and the user of interest, we obtain an average NMSE of -18 dB outside the CP region.

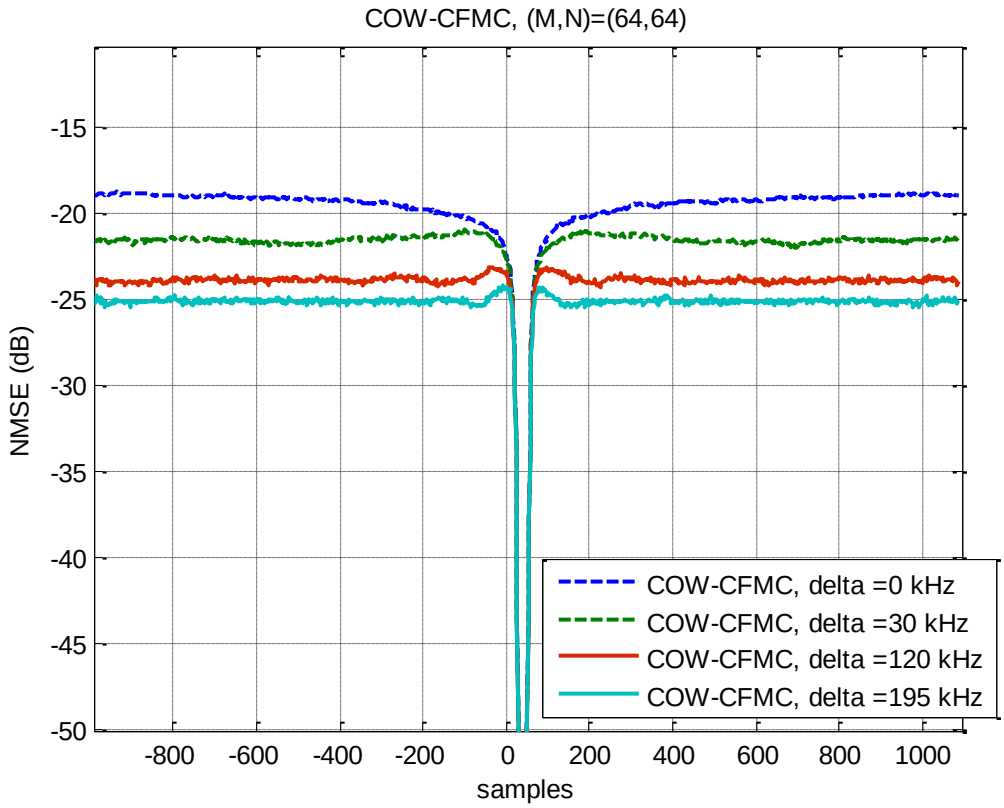

Figure 10: Average NMSE against timing offset (samples).

5.4.2 Carrier frequency offset (CFO)

In this subsection, we assume that both users are perfectly synchronized in time domain but there is an offset between their respective carrier frequencies. The objective here is to examine the impact of inter-user interference induced by CFO on the performance of COW-CFMC waveform. The CFO considered here varies from −1.5kHz to +1.5kHz. Multiple guard-band sizes are also considered as: $\delta = 0, 30, 120\ 195$ kHz.

In Fig. 11, we have the per-subcarrier MSE of COW-CFMC system. We observe that the edges subcarriers are more sensitive to CFO compared to inner ones. In fact, the MSE at the edges becomes important even for negligible CFO (from 150Hz) while inner subcarriers keep best performances (MSE < −30dB) even when *CFO is* 1.5kHz.

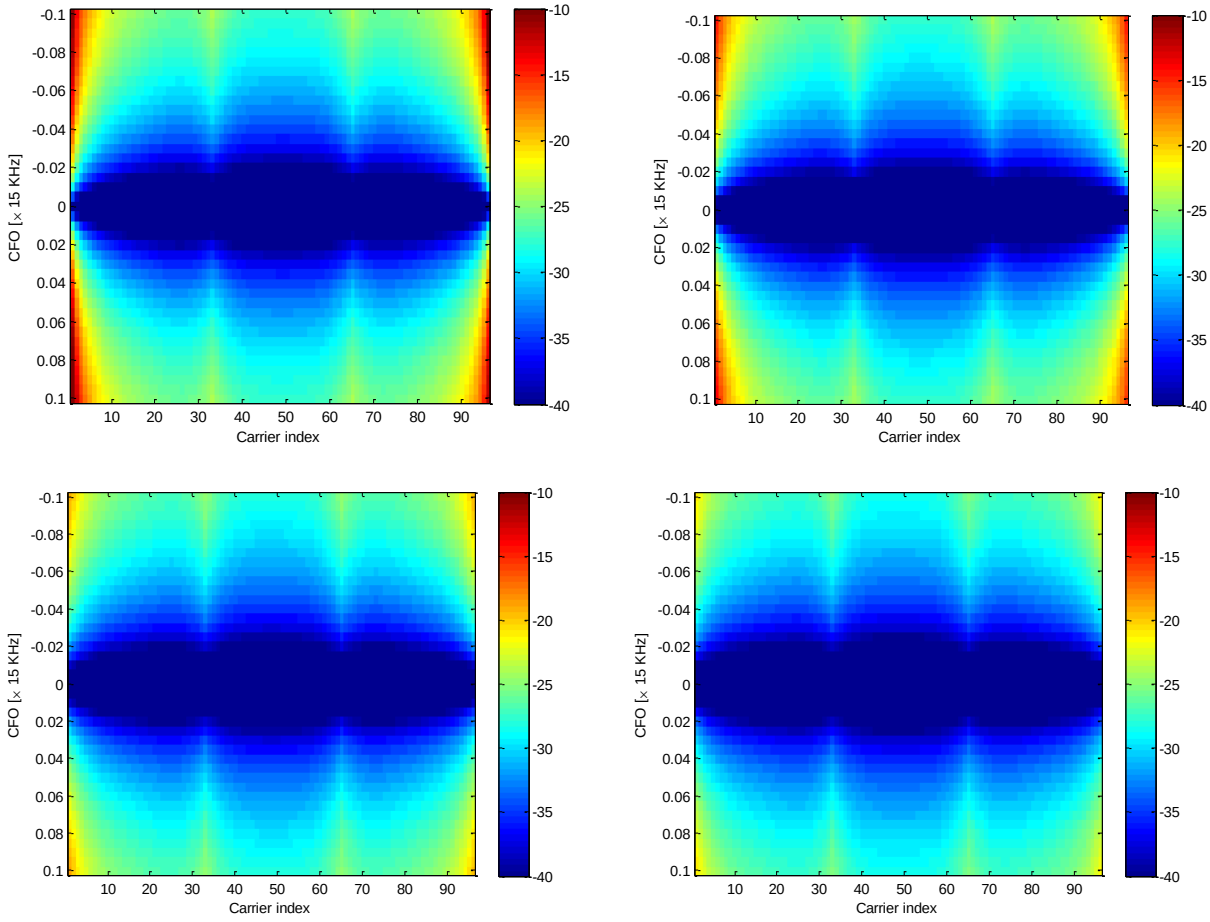

Figure 11: per-subcarrier NMSE against CFO.

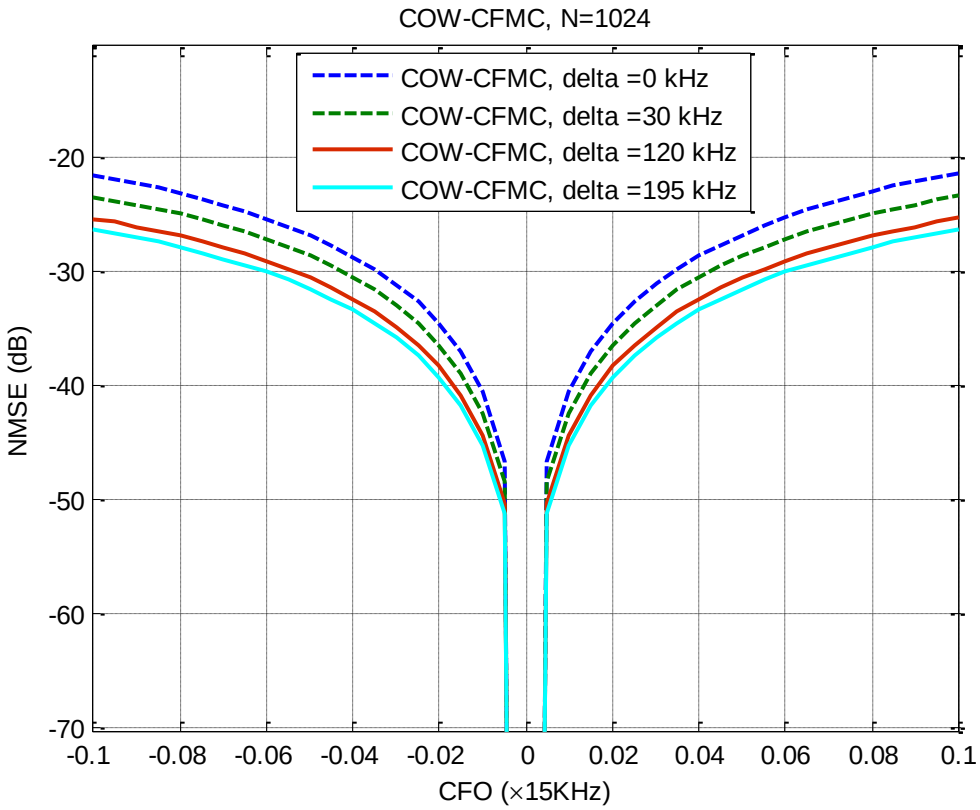

Figure 12: average NMSE against CFO

The average NMSE of COW-CFMC computed over all subcarriers is plotted in Fig. 12, as function of CFO considering various guard-bands: $\delta = 0, 30, 120$ 195 kHz. Looking at the NMSE curves, we can notice that the proposed COW-CFMC waveform is strongly sensitive to CFO. That is, the NMSE rapidly grows to -26 dB when CFO varies from 0 to 1.5 KHz.

6 Serving Spatially Clustered D2D Scenarios using different waveforms

In this section, we focus on two enabling technologies: D2D communications and enhanced waveforms. Enhanced waveforms with improved spectral localisation over orthogonal frequency division multiplexing (OFDM) as they can enable asynchronous communication between devices, and hence reduce the control overhead associated with achieving synchronism. In contrast, OFDM's strict synchronicity requirements makes it unsuited to asynchronous communications with its large side lobes resulting in significant leakage.
In the context of the type of 5G scenarios under consideration, two additional benefits are obtained by using an enhanced waveform to enable asynchronous communications between clustered D2D user equipment (DUE). First, we wish to enable 5G network operators to serve spatially clustered D2D use cases with minimal additional control overhead. Removing the requirement for the BS to synchronise DUEs would permit the network operator to treat resource allocation for high-rate clustered D2D scenarios in a different manner than for Cellular user equipment (CUEs).

In this deliverable, we expand upon our previous work in [17], which demonstrated the effects of inter-D2D interference arising from misaligned communications in a spatially clustered single-cell scenario, and how the use of a waveform that exhibits improved spectral localization over OFDM can mitigate this interference. We investigate whether the use of enhanced waveforms cellular networks can provision high-rate, latency-intolerant clustered D2D applications using minimal additional control. We also consider a network consisting of cells which employ strict fractional frequency reuse (FFR).

We build upon our work in [18], which provides interference tables capturing the effects of misaligned D2D users in time onto OFDMA-based cellular users in the uplink band. We also draw upon the work of [19] and [20] in order to characterize the interference imposed between entities utilizing different waveforms. We perform system-level simulations in order to

evaluate the relative performance of several waveforms for use in the type of clustered D2D scenarios outlined in this section.
We also investigate how the level of asynchronism between devices affects the SINR performance of DUEs, examining the effects of both timing offset (TO) and carrier frequency offset (CFO). We stress that our interest lies in investigating the relative performance of different waveforms in such a scenario; we are not concerned with developing a new resource allocation scheme for underlay D2D, of which there are many in the literature. The main contributions of this section are the following:

- _We rate, with a high level of accuracy, the interference arising from the asynchronous coexistence between a large number of enhanced waveforms. We then use the tabulated interference values in system-level simulations.
- _We demonstrate that it is feasible for cellular networks to serve high-rate clustered D2D use cases through a coexistence of enhanced waveforms and OFDM, and quantise the benefit of doing so.
- _We characterize the performance of several prominent enhanced waveforms across a range of scenarios by varying key system parameters such as cell size, cluster size, DUE transmit power, and maximum possible timing offset and CFO.

6.1 System model

We stay consistent with the literature and consider uplink resource sharing for two reasons. Firstly, interference from DUEs experienced by cellular users occurs at the base station. Therefore, the BS can attempt to coordinate and mitigate this interference through resource allocation schemes. Secondly, and more importantly, DUEs should not interfere with crucial pilot information broadcast in the downlink. We consider an OFDMA network with parameters selected based on the 3GPP LTE standard, as outlined in Table 2. CUEs are distributed throughout the entire network according to a Poisson point process (PPP). DUEs are employed in high-rate spatially clustered applications. We distribute DUE transmitters in the network using a Matérn point process which generates clusters according to a two-step process. In the first step, a PPP is used to generate a set of parent points. In the second step, a Poisson distributed number of child points is uniformly distributed around each parent point within a disk of a given radius. The rate of occurrence of clusters, DUE transmitters per clusters, and the cluster radii can be configured in the simulation parameters. For each DUE transmitter, we distribute a receiver at a distance d according to a uniform random variable U[a;b], with a and b representing the minimum and maximum distance, respectively.
The ratio of the radius of the inner region (R_{inner}) to the radius of the cell (R_{cell}) is an important parameter in strict FFR systems and influences how sub-bands are divided between regions. We follow the approach used in [21], and choose the ratio R_{inner}=R_{cell} to be 0:65, which was shown in [19] to maximise the average network throughput for uniformly distributed CUEs. Given N_{band} available sub-bands in the system, we can determine the number of resources allocated to each region as follows [22]

$$N_{inner} = \left[N_{band}\left(\frac{R_{inner}}{R_{cell}}\right)\right]$$
$$N_{outer} = \left[\frac{(N_{band} - N_{inner})}{3}\right]$$

RBs are assigned under the condition that an RB may only be assigned to a single CUE, and reused by a single DUE, in a given cell. CUEs transmit on the physical uplink shared channel (PUSCH) and use a power control procedure that assigns each CUE a power level that results in acceptable signal reception at the base station. Our focus in this paper is on evaluating the relative performance of enhanced waveforms for asynchronous direct communication between devices/equipment in spatially clustered use cases, not on proposing a new resource allocation scheme.

6.1.1 Channel Modelling

CUEs in the same cell do not interfere with each other, as we assume they are perfectly synchronized by the BS. Therefore, there are four main interference types requiring consideration:

1) DUE pairs interfere with the CUEs' transmissions. Since
1. we are investigating uplink resource sharing, this interference is observed at base stations.
2. Conversely, the CUEs interfere with the DUE pairs at DUE receivers.
2) DUEs interfere with each other (inter-DUE interference).
3) CUEs in different cells are not synchronized and, hence, interfere with each other (inter-CUE interference).

Owing to their popularity in the existing literature [23], [24], [25], we employ the WINNER II channel models [26] to provide us with a distance based path loss, which also incorporates the probability of line-of-sight. Distinct path loss models are used for the different types of links in the system in order to represent the network in a realistic manner. Path loss models employed for D2D channels have been modified so that the elevation of transceivers terminating a common

link are comparable. The distribution of shadow fading is lognormal, with the standard deviation specified by the Winner II channel models for each scenario.

6.1.2 Performance Measures

we present several∈d details of their formulation that we will use to evaluate the performance of the system. All metrics are evaluated for DUEs and CUEs in the central cell, which represents the cell of interest.
1) SINR: The SINR of a CUE *j* in the central cell o using RB *k* is given by:

$$\gamma_{j_o}^{k} = \frac{P_{j_o}^{k} h_{j_o B}^{k}}{\sigma_v^2 + I_{C_N} + I_{D_N} + I_{D_S}}$$

where $P_{j_o}^{k}$ is the transmit power of the CUE, $h_{j_o B}$ is the channel gain between the j^{th} CUE and the BS of the central cell *o*, and σ_v^2 is additive white Gaussian noise variance. I_{C_N} is the interference from CUEs in neighbouring cells and is given by

$$I_{C_N} = \sum_{n \in N} \sum_{c_n \in C_N} \sum_{r \in R} \omega_{r c_n} P_{C_n}^{r} \; h_{C_n B}^{r} \; \Omega_{wf_{c_n} \rightarrow wf_{j0}} \; (|r-k|, \delta_t, \delta_f)$$

where *n* indexes the set of neighbouring cells *N*, c_n indexes the CUEs in the set C_n of CUEs in the *n-th* neighbouring cell, and *r* indexes the set of resource blocks *R* available to the system. $P_{C_n}^{r}$ is the transmit power of the $c^{th}{}_n$ CUE operating on RB *r*, $h_{C_n B}^{r}$ is the channel gain between the $c^{th}{}_n$ CUE and the BS of the central cell, and $\omega_{r c_n}$ is a resource reuse indicator where $\omega_{r c_n} = 1$ when CUE c_n uses RB *r*, and $\omega_{r c_n} = 0$ otherwise.
Finally, $\Omega_{wf_{c_n} \rightarrow wf_{j0}} \; (|r-k|, \delta_t, \delta_f)$ is the fraction of power injected by CUE c_n using waveform wf_{c_n} and resource block *r* onto CUE j_o using waveform wf_{j0} and resource block *k*, at a timing offset of δ_t and cfo δ_f. I_{D_N} is the interference from DUEs in the neighbouring cells and is given by

$$I_{D_N} = \sum_{n \in N} \sum_{c_n \in C_N} \sum_{r \in R} \omega_{r d_n} P_D \; h_{d_n B}^{r} \; \Omega_{wf_{d_n} \rightarrow wf_{j0}} \; (|r-k|, \delta_t, \delta_f)$$

which is defined in a similar fashion than in I_{C_N}, where D_n represents the set of DUEs in the n^{th} neighbouring cell, and P_D is the transmit power of DUE devices. Finally, I_{D_S} represents the interference from DUEs in the same cell, i.e. the central cell, and is formulated in a similar fashion as for I_{D_N}. The SINR of a DUE d in the central cell o operating on RB *r* is given by:

$$\gamma_{d_o}^{r} = \frac{P_D \; h_{d_o}^{r}}{\sigma_v^2 + I_{C_N} + I_{C_S} + I_{D_S} + I_{D_N}}$$

where $h_{d_o}^{r}$ is the channel gain between the transmitter and receiver of the d^{th} DUE using RB *r*. I_{C_S} and I_{C_N} represent the aggregate interference from CUEs in the same cell and neighbouring cells, respectively. I_{D_S} and I_{D_N} represent the aggregate interference from DUEs in the same cell and neighbouring cells, respectively.

2) Achieved Rate: We are also interested in the rate achieved by devices, after the bandwidth efficiency of each waveform has been taken into account. The rate of a device using a waveform wf can be calculated as

$$b = \Phi_{\text{wf}} \, B \log_2(1+\gamma) \; [b/s]$$

where *B* is the bandwidth of an LTE resource block, and Φ_{wf} is the bandwidth efficiency of waveform wf presented in Table 1, which is directly computable based on the waveform parameters presented in Table 2.

Table 1: Bandwidth Efficiency of Waveforms [1]

Waveform	Bandwidth Efficiency (Φ_{wf})
OFDM	8/9
FMT	8/9
GFDM	5/(5 + 1/8)
FBMC/OQA	11/12
FBMC-PAM	11/12
F-OFDM	8/9 ∗ 11/12
UFMC	8/9

[1] Detailed information on advanced waveforms can be found in [28] and [29]

6.2 Evaluation and system performances

We first present detailed results for the case defined by the parameters listed in Table III. We then examine how the performance of the system changes depending on the scenario by varying a key parameter of interest while maintaining the other parameters as per their value in Table 2.
The cell radius value of 250m is based on the 3GPP LTE system scenarios [27], representing an urban macro-cell environment. The antenna gain values, noise figures, and the carrier frequency value are also based on [27]. The values for the maximum CUE transmit power, subcarrier spacing, and number of resource blocks are based on the LTE standard, with 50 resource blocks corresponding to a bandwidth of 10MHz. The maximum DUE transmit power of 0 dBm was chosen as it was found through experimentation to yield good results. The effects of varying the maximum DUE transmit power will be discussed later in this section.
We explore the case whereby each macro-cell is fully loaded and hence consider a large number of CUEs per square kilometer to ensure this. The parameters relating to the size and frequency of occurrence of clusters are scenario dependent.

A cluster of radius 60m, containing 30 inter-communicating devices and with an average of 3 clusters per square kilometer might, for example, represent a factory in an urban area with moderate industrial activities. For each of the candidate waveforms, we investigate two cases:

1) Case 1: DUEs pairs deploy waveforms from the pool of waveforms under study, CUEs use OFDM.
2) Case 2: Both DUE pairs and CUEs deploy waveforms from the pool of waveforms under study.

We also examine the effects of the timing offset on the relative performance of waveforms, ranging from perfectly synchronised to fully asynchronous communication. Scenarios whereby DUEs achieve coarse synchronization with a stated maximum permitted timing offset are of interest, and accordingly investigated for different ranges of maximum permitted offsets. An analogous investigation is performed for CFO by varying local oscillator (LO) inaccuracies.

Table 2: Simulation parameters

Parameter	Value
Cell Radius	250 m
Inner Radius	163 m
Number of Cells	19
CUEs Per Square Km	200
DUEs Per Cluster	30
Clusters Per Square Km	3
Average Cluster Radius	60 m
Average Tx Rx Distance	Uniformly distributed in the range [10, 50] m
Carrier Frequency	2 GHz
Subcarrier Spacing (Δf)	15 kHz
Noise Per RB [2] (σ^2_v)	-116 dBm
Number RBs in system	50
$P_{O\ PUSCH}$	-96 dBm
α	1
Max Tx Power CUE	24 dBm
Max Tx Power DUE	0 dBm
BS Antenna Gain	15 dBi
UE Antenna Gain	0 dBi
BS Noise Figure	5 dB
UE Noise Figure	9 dB
Max Timing Offset	$T + T_{CP}$
Max Local Oscillator (LO) Inaccuracy	2.5 ppm
Waveforms [28] [29]	OFDM, FMT, FBMC/OQAM, FBMC-PAM, GFDM, f-OFDM, UFMC
Number of Iterations	5000

Figure 13 presents box plots summarizing the SINR distribution for DUEs according to each considered waveform couple. Several choices comprising enhanced waveforms offer significantly better results than the sole use of OFDM, with

FBMC/OQAM, FBMC-PAM, f-OFDM, and FMT each providing significant performance boosts. The best performance is achieved when both CUEs and DUEs use one of the aforementioned enhanced waveforms.
Encouragingly, performance increases are also possible in coexistence scenarios whereby CUEs use OFDM and DUEs use an enhanced waveform. For example, in the case whereby CUEs use OFDM and DUEs use FBMC/OQAM, a performance increase of approximately 9dB can be obtained when compared to the case where both sets of users employ OFDM. We note that the number of outliers is relatively small (approx. 2:2%) compared to the number of DUEs in the data set.

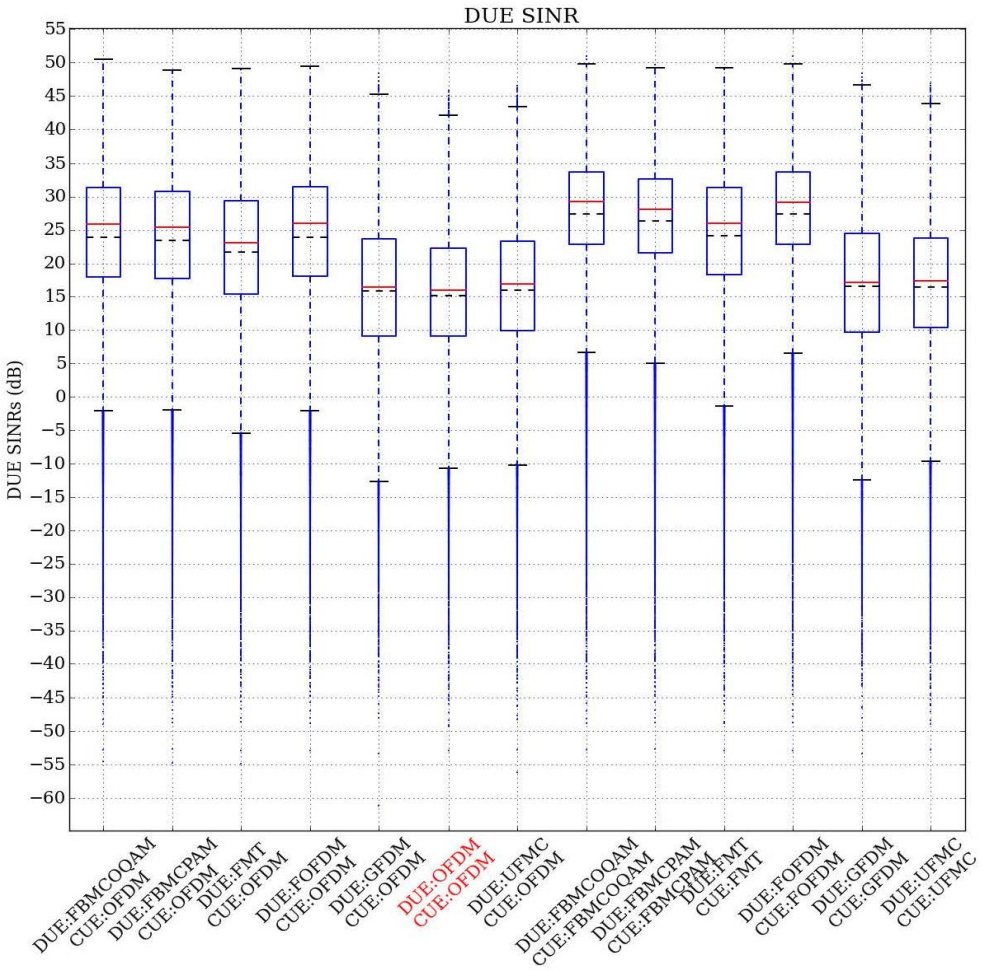

Figure 13: The box plots of DUE SINR show that a large performance increase can be obtained by choosing an appropriate enhanced waveform.

We also wish to show the achieved rate of DUEs, taking into account the bandwidth efficiency of each modulation scheme. Figure 14 shows the achieved rate of DUE pairs for each waveform. We again note that the greatest performance increase is achieved when both CUEs and DUEs use an enhanced waveform in the set {FBMC/OQAM, FMT, FBMC-PAM, f-OFDM}.
In the coexistence scenarios, in which CUEs use OFDM and DUEs use an enhanced waveform in the set {FBMC/OQAM, FMT, FBMC-PAM, f-OFDM}, there is a slight variation in the achieved rate despite the fact that each waveform yielded a similar SINR performance in Figure 13.

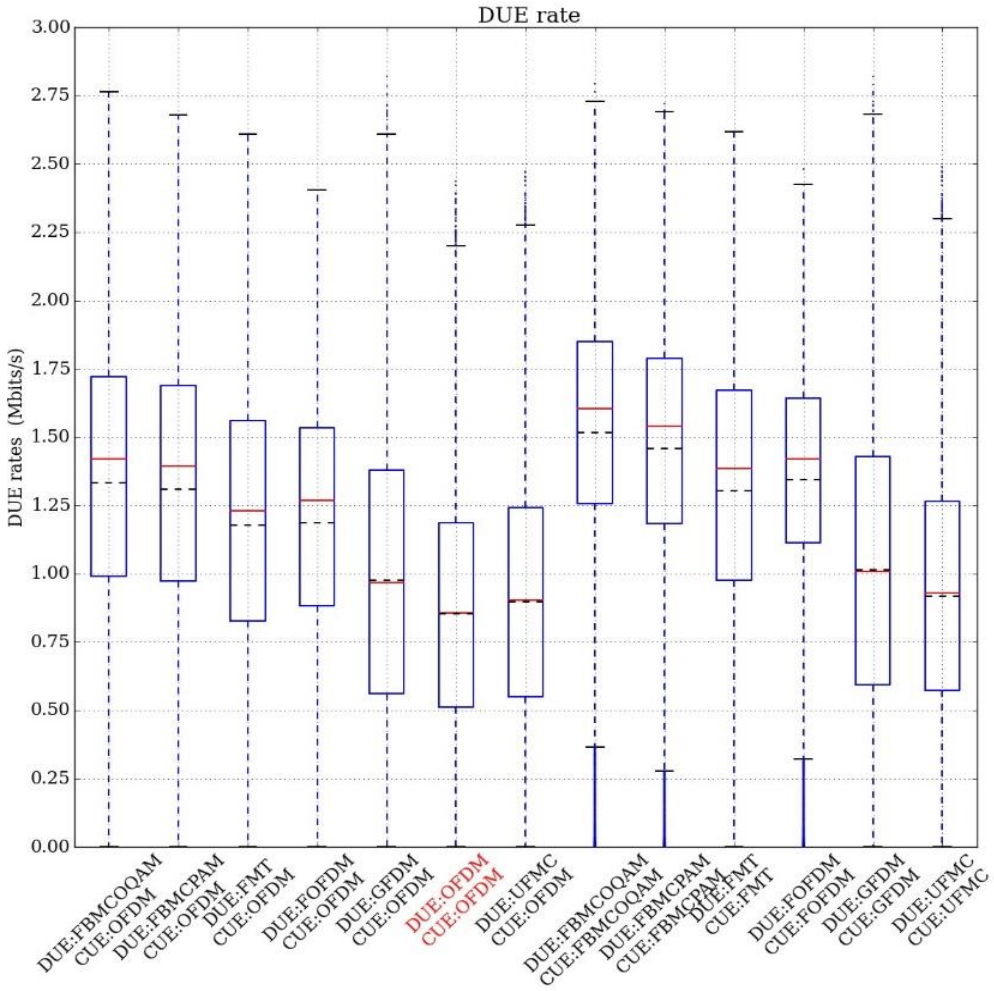

Figure 14: Rate performance of DUEs taking into account bandwidth efficiency.

6.2.1 Cell Radius

In this subsection, we investigate the influence that cell radius has on performance by varying the cell radius from 200m to 1000m in 100m increments while holding all other parameters at the same value as in Table III. We display the results in Figure 15 For cell radii under 500m, we consider an urban environment and use the appropriate path loss models for this scenario, while for cell radii greater than 500m, we consider a suburban environment. At the smallest cell radius considered (200m), average DUE SINR is at its lowest and average DUE to CUE interference is at its greatest. This is understandable, and readily explained.
According to the strict FFR scheme employed, DUEs reuse the resources of CUEs in neighbouring reuse regions. At smaller cell sizes, the average distance between devices in neighbouring reuse regions is reduced. This results in greater CUE to DUE interference and reduces DUE SINR. As the cell radius increases, so too does the distance between reuse regions, and DUE SINR increases. This increase is mainly observed at smaller cell sizes; at large cell sizes, CUE to DUE interference is almost negligible and further increases to cell radius exhibit little or no increase in DUE SINR.

DUE to CUE interference, on the other hand, occurs at base stations. In smaller cells, the average distance between clusters and the base stations serving neighbouring reuse regions is shorter, resulting in higher DUE to CUE interference. This is evidenced in the lower sub-plot in Figure 15, in which we observe that the average DUE to CUE interference decreases as the cell radius increases. Therefore, as the cell size increases, average DUE to CUE interference decreases and average DUE SINR increases. Essentially, the greater the cell size the more protection strict FFR offers against the various types of interference, as the reuse regions are further apart.
We note at the maximum cell radius considered (1000m), f-OFDM and FBMC/OQAM both offer approximately an 11dB improvement in the coexistence scenario over the base-line OFDM-OFDM case. At large cell sizes, even further gains are achievable as DUEs could transmit at a higher power without affecting CUEs. Unfortunately, at the other end of the scale, DUEs in very small cells might not be able to transmit at a power level that allows them to obtain the required data

rates without interfering too much with CUEs. In these cases, additional measures may need to be developed and deployed to enable DUE communication, such as advanced resource allocation schemes that minimize the interference from DUEs to CUEs. Failing that, DUE communication may only be permitted to underlay sufficiently large cells

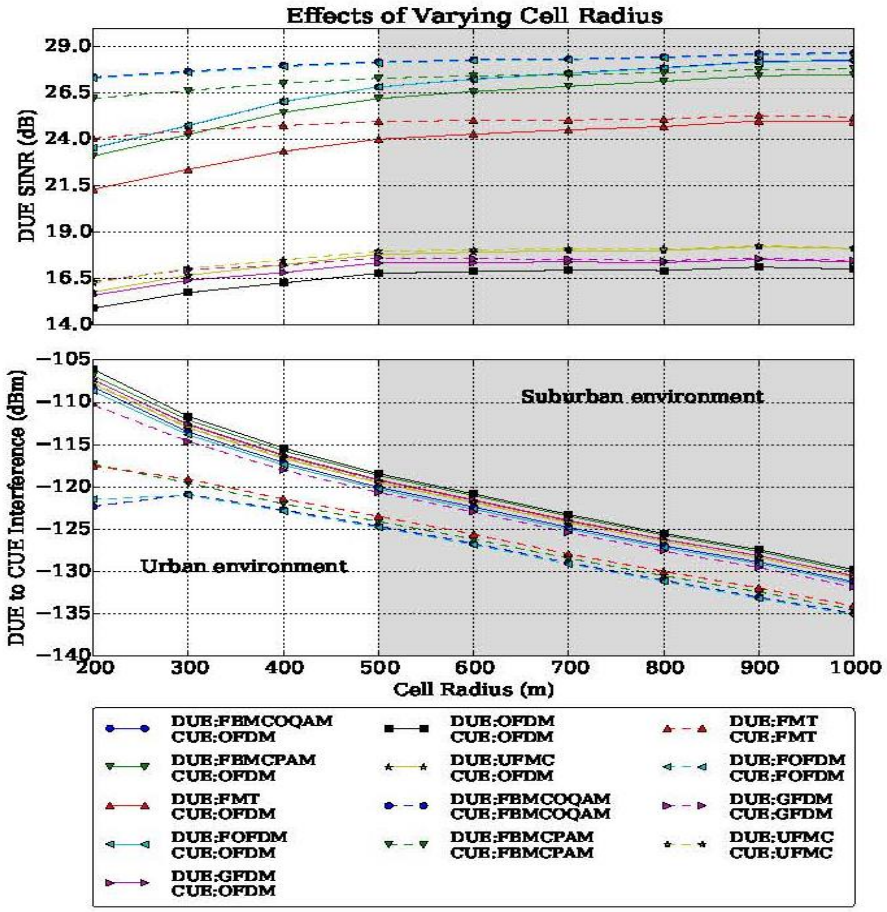

Figure 15: As the cell radius increases, DUE SINR increases and reduction in CUE SINR decreases.

6.2.2 Cluster Radius

We investigate the impact that cluster radius has on performance. We present the results in Figure 16, varying the cluster radius from 30m to 100m in 10m increments. Reducing the cluster radius necessitates a corresponding change in the distance between a DUE transmitter and receiver, which we modelled using a uniform random variable. Accordingly, we choose the parameters a and b of the uniform random variable $U_{[a;b]}$ as follows: a = 5; b = (cluster radius) - 10. Increasing the cluster radius has two opposing influences on DUE SINR. On the one hand, it results in reduced inter- DUE interference, which should boost the SINR. On the other hand, it also results in reduced received signal power, which should cause the SINR to decrease. This makes it difficult to predict how the average SINR will change. In Figure 16, we see that the reduction in received power is more influential and however, that this is somewhat dependant on how the distance between DUE transmitters and receivers is modelled (such as the parameters a and b), as this affects by how much the received power will decrease. We also note that for small cluster sizes, and in cases where DUEs do not use a waveform in the set {FBMC/OQAM, FMT, FBMC-PAM, f-OFDM}, SINR decreases slowly at first as the reduction in inter-DUE interference is almost significant enough to counter-act the effect of lower received signal powers.

Reducing the cluster radius increases the density of DUEs in the cluster, resulting in greater inter-DUE interference. Hence, employing an appropriate enhanced waveform for DUEs yields the greatest benefit in dense clusters in which inter-DUE leakage interference is most significant.

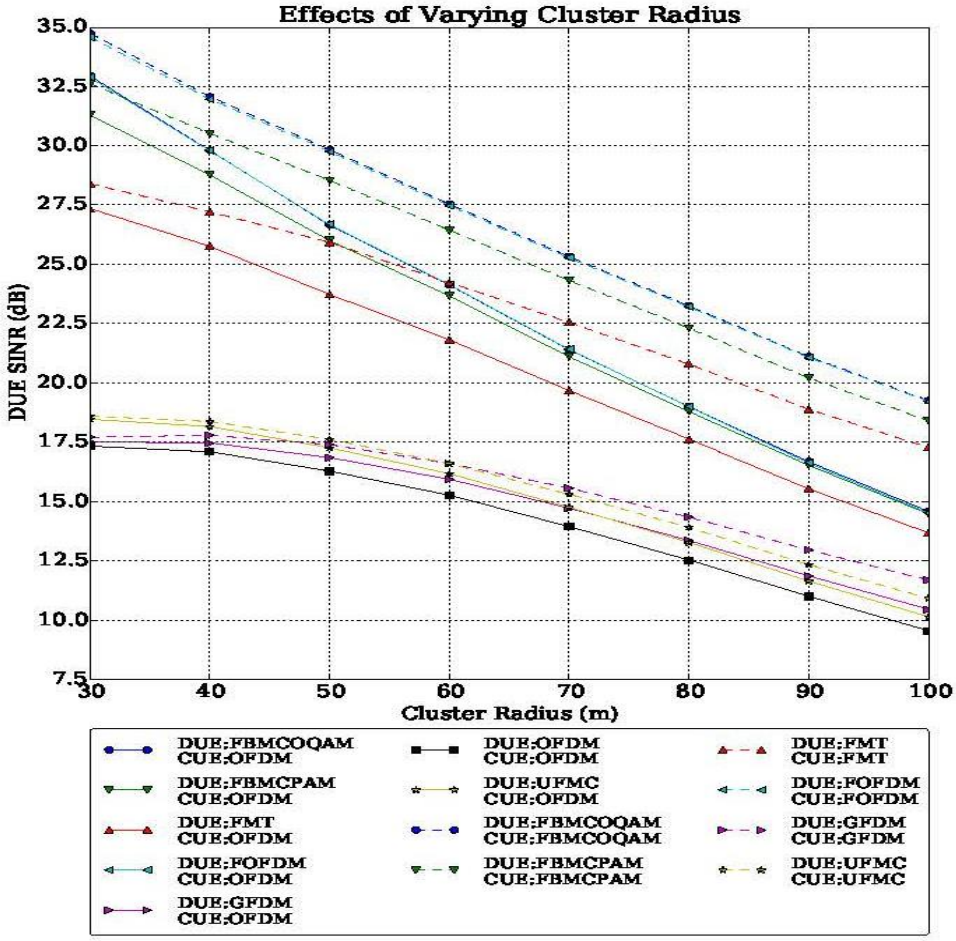

Figure 16: Employing an appropriate enhanced waveform for DUEs yields the greatest benefit in small clusters in which inter-DUE leakage interference is most significant.

6.3 Summary

We demonstrated that, due to the spatially clustered nature of communication in the type of scenarios being considered, inter-DUE leakage interference plays a prominent role and significant benefits can be obtained in certain scenarios by utilising enhanced waveforms. The benefit of using a spectrally contained waveform is largely restricted to DUEs, which operate asynchronously and in close proximity to one another, and not the CUEs. We demonstrated that the greatest benefits are obtained when both CUEs and DUEs both use an appropriate enhanced waveform.
We showed that system performance is parameter dependent. In an urban environment, DUEs can enjoy high SINRs without greatly affecting the performance of cellular users; improvements in excess of 9dB are attainable in cells of radius 250m and greater. However, for smaller cells, strict FFR may not offer enough protection to CUEs from interference caused by DUEs, and additional measures may be needed to reduce interference to CUEs if DUEs are to transmit with a power level that permits them to achieve reasonable performance.

7 Optimal Power Allocation for Full Duplex D2D Communication

With the rapidly growing of customers data traffic demand, improving the system capacity and increasing the user throughput have become essential concerns for the future wireless communication network, i.e. 5G. In this context D2D communication and Full Duplex (FD) are proposed to increase the spatial spectrum utilization and the user rate in cellular network [30]. D2D allows two nearby devices to communicate without base station participation or with a limited participation. On the other hand, FD communication allows simultaneous transmission and reception in the same frequency band. Hence, it will enhance the spectral efficiency of a single peer-to-peer channel and improve the user throughput (potentially doubled) over the conventional half-duplex (HD) communication [31].

The main challenge in FD communication is the strong self-interference (SI) imposed on the receiver by the transmitter of the same node [32]. However, the recent works on FD show that huge advances have been made in mitigating the SI, and the respective state of the art of transceiver design can achieve a high level of self-interference cancellation (SIC) [33][34]. Hence, the FD technology has become closer to be applied in the new wireless cellular network.

The short distance property of the D2D link makes the transmission power of the D2D users relatively lower. Thus, exploiting the FD transmission in D2D communication is an excellent choice to furthermore improve the cellular spectrum efficiency and the user throughput [35]. However, the full duplex D2D (FD-D2D) communication adds new challenges for the D2D communication. For example, the amount of SI is highly depending on the transmitted power value. Thus, the power allocation strategy in FD-D2D is a very important problem to be tackled.

The authors of [38] derived and analysed a closed form expression of the sum-rate of FD-D2D underlay cellular network. However, in their work the optimal power allocation scheme was not discussed and they assumed a symmetric scenario where the D2D users have the same distance from the base station and the CUE has equal distance to the D2D users. The power optimization problem of an isolated FD-D2D pair underlay cellular network was tackled in [36]. Unlike [36], the authors of [37] derived a convex optimization problem to maximize the rate of FD-D2D link while satisfying the minimum rate requirement of the cellular users. Although the solution derived in [37] is not limited by the case where the distances between the D2D users and the CUE is equal, the authors of [37] neglected the effect of the CUE location w.r.t the D2D users and they did not clearly described the D2D pair situation in their numerical results. Moreover, neither [36] nor [37] provided a mathematical expression for the optimal power allocation scheme.

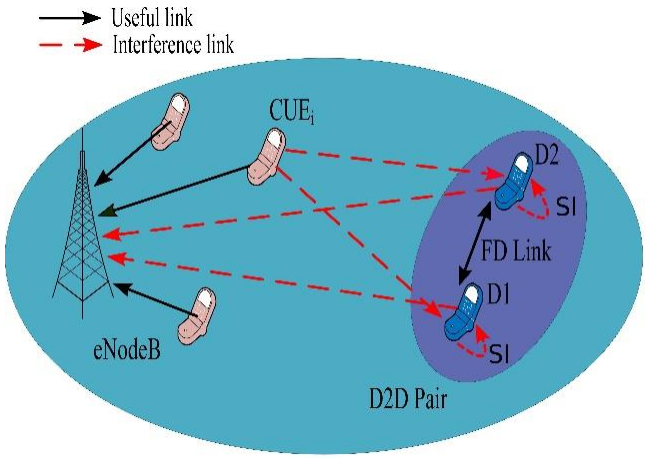

Figure 17: A FD-D2D pair shares the resources of one cellular user, which creates interference between the two types of links.

7.1 System model

As depicted in Figure 17, we consider a FD-D2D enabled cellular network. The cellular network consists of an eNodeB, one D2D pair and multiple CUEs. The CUEs are allocated orthogonal sub-channels for uplink transmission and they are assumed to be operated in HD mode. While the FD-D2D users can share only one uplink sub-channel during their transmission so there is interference only between one cellular user (CUE_i in Figure 17) and the D2D pair.
Although the advanced transceiver designs can significantly decrease the SI, in practical scenario it is impossible to totally delete it. In this work, the power of the residual self interference (P_{RSI}) is defined as follows:

$$P_{RSI} = \eta P_t \qquad (40)$$

where η ($0 \leq \eta \leq 1$) is the SI mitigation coefficient which represents the effect of the advanced SIC techniques [36] [37], and P_t is the local transmit power. The case of $\eta = 0$ corresponds to the perfect SIC while $\eta = 1$ reflects the invalidity of SIC. To model the cellular/FD-D2D links as well as the interference links, both the distance based path-loss model and the fast fading model are considered. Thus the channel gain between a transmitter i and a receiver j can be expressed as $g_{ij} = l_{ij} h_{ij}$, where l_{ij} denotes the path-loss attenuation and h_{ij} stands for the Rayleigh distribution fading coefficient with unit mean power gain (i.e. $h_{ij} \sim \exp(1)$). Furthermore, the path-loss attenuation can be expressed by $l_{i,j} = d^{-a}$ where ''a'' is the standard path loss exponent and d is the distance between the transmitter i and the receiver j. Considering an interference

limited system as in [38] [39], i.e. assuming the receiver noise as negligible, the instantaneous Signal-to-Interference ratio (SIR) of the CUE, the first D2D user (D1) and the second D2D user (D2) can be respectively expressed as:

$$\gamma_c = \frac{P_c\, l_{c,BS}\, h_{c,BS}}{P_{d1}\, l_{d1,BS}\, h_{d1,BS} + P_{d2}\, l_{d2,BS}\, h_{d2,BS}} \quad (42)$$

$$\gamma_{d1} = \frac{P_{d2}\, l_d\, h_{d2,d1}}{P_c\, l_{c,d1}\, h_{c,d1} + \eta P_{d1}} \quad (43)$$

$$\gamma_{d2} = \frac{P_{d1}\, l_d\, h_{d1,d2}}{P_c\, l_{c,d2} h_{c,d2} + \eta P_{d2}} \quad (44)$$

where P_c, P_{d1} and P_{d2} are respectively the transmit powers of the *CUE*, *D*1, and *D*2.

7.2 Ergodic capacity analysis

In this subsection, we will first provide a new closed form expression for the ergodic capacity of a FD-D2D link (R_{FD}) which is using the CUE uplink resources. R_{FD} is defined as the summation of *D*1's and *D*2's ergodic capacities, R_{D1} and R_{D2} in (45), and it is given by:

$$R_{FD} = \underbrace{\mathbb{E}_{\gamma_{d1}}[\log_2(1+\gamma_{d1})]}_{R_{D1}} + \underbrace{\mathbb{E}_{\gamma_{d2}}[\log_2(1+\gamma_{d2})]}_{R_{D2}} \quad (45)$$

where γ_{d1} and γ_{d2} are the SIRs given by (43) and (44) respectively. $\mathbb{E}(:)$ denotes the expectation operation. From (45), in order to derive the FD ergodic capacity, the probability density function (PDF) of the SIRs must be calculated. The following Lemmas provide such PDFs.

Lemma 1. The distribution of the CUE SIR is given by:

$$f_{\gamma_c}(t) = \left(\frac{P_c\, l_{c,BS}}{P_{d1} l_{d1,BS} - P_{d2} l_{d2,BS}}\right) \left[\frac{(P_{d1} l_{d1,BS})^2}{(tP_{d1} l_{d1,BS} + P_c l_{c,BS})^2} - \frac{(P_{d2}\, l_{d2,BS})^2}{(tP_{d2} l_{d2,BS} + P_c l_{c,BS})^2}\right] \quad (46)$$

Proof: First let us define the two following random variables $X = P_c\, l_{c,BS}\, h_{c,BS}$ and $Y = P_{d1}\, l_{d1,BS}\, h_{d1,BS} + P_{d2}\, l_{d2,BS}\, h_{d2,BS}$. The channel power gains follow the exponential distribution. Therefore, the PDF of X and Y are $\frac{1}{P_c l_{c,BS}} e^{-\frac{x}{P_c l_{c,BS}}}$ and $\frac{e^{-\frac{y}{P_{d1} l_{d1,BS}}} - e^{-\frac{y}{P_{d2} l_{d2,BS}}}}{P_{d1} l_{d1,BS} - P_{d2} l_{d2,BS}}$ respectively.
By defining new variables *S*= *Y* and T = X/Y and applying the change of variable theorem, the joint PDF for the couple (*S; T*) can be written as:

$$f_{ST}(s,t) = f_{XY}(X(s,t), y(s,t))|J(s,t)| = \frac{s e^{\frac{-st}{P_c l_{c,BS}}}}{P_c l_{c,BS}} \left[\frac{e^{-\frac{s}{P_{d1} l_{d1,BS}}} - e^{-\frac{s}{P_{d2} l_{d2,BS}}}}{P_{d1} l_{d1,BS} - P_{d2} l_{d2,BS}}\right] \quad (47)$$

where $|J(s,t)|$ is the Jacobian of the transformation. Now, integrating (47) w.r.t s completes the proof Lemma 2. The PDF of the *D*1 and *D*2 SIRs are given by:

$$f_{\gamma_{d1}}(t) = e^{t\frac{\eta P_{d1}}{P_{d2} l_d}} \left(\frac{(P_{d1} P_c\, l_d\, l_{c,d2} + \eta\, P_{d1} P_{d2}\, l_d + t\,\eta\, P_c P_{d1} l_{c,d1})}{(tP_c l_{c,d1} + P_{d1} l_d)^2}\right. \quad (48)$$

$$f_{\gamma_{d2}}(t) = e^{t\frac{\eta P_{d2}}{P_{d1} l_d}} \left(\frac{(P_{d2} P_c l_d l_{c,d1} + \eta P_{d1} P_{d2} l_d + t\eta P_c P_{d2} l_{c,d2})}{(t P_c l_{c,d2} + P_{d1} l_d)^2} \right. \tag{49}$$

Proof: The PDF of γ_{d1} and γ_{d2} can be obtained by following the same procedure as in Lemma 1. Now, putting the D2D SIR distributions derived in Lemma 2 in (45) and integrating the Shannon capacities over the SIRs leads to the following theorem : Theorem 1. The full duplex ergodic capacity is given by:

$$R_{FD} = \underbrace{\frac{E_1\left(\frac{\eta x}{l_{c,d1}}\right) e^{\frac{\eta x}{l_{c,d1}}} - E_1\left(\frac{\eta x}{l_d y}\right) e^{\frac{\eta x}{l_d y}}}{\frac{l_{c,d1}}{l_d y} - 1}}_{R_{D1}} + \underbrace{\frac{E_1\left(\frac{\eta y}{l_{c,d2}}\right) e^{\frac{\eta y}{l_{c,d2}}} - E_1\left(\frac{\eta y}{l_d x}\right) e^{\frac{\eta y}{l_d x}}}{\frac{l_{c,d2}}{l_d x} - 1}}_{R_{D2}} \tag{50}$$

Where $x = \frac{P_{d1}}{P_c}, y = \frac{P_{d2}}{P_c}$ and $E_1(z) = \int_z^\infty \frac{e^{-t}}{t} dt$ is the first order exponential integral. Note that the function

$$h(x) \triangleq \exp\left(\frac{1}{x}\right) E_1\left(\frac{1}{x}\right) \tag{51}$$

is a monotonically increasing function with x [40]. Accordingly, for a > b (a and b are arbitrarily positive numbers)

$$\exp\left(\frac{\eta y}{a}\right) E_1\left(\frac{\eta y}{a}\right) > \exp\left(\frac{\eta y}{b}\right) E_1\left(\frac{\eta y}{b}\right)$$

then we have (52)

$$\frac{b}{a-b}\left[e^{\frac{\eta y}{a}} E_1\left(\frac{\eta y}{a}\right) - e^{\frac{\eta y}{b}} E_1\left(\frac{\eta y}{b}\right)\right] > 0 \tag{53}$$

The same result can be obtained for a<b. Thus, R_{D1} and R_{D2} are always positive and monotonically increasing with respect to y and x respectively. This in turn verifies that the FD capacity derived in (50) is always positive. In FD communication the D2D users share the whole CUE's spectrum while in HD only one D2D user can use the CUE's resources. Thus, for fair comparison R_{HD} is assumed to be the maximum of the HD rate of $D1$ and $D2$ as presented in (54).

$$R_{HD} = \max\left(\underbrace{\frac{\log_2\left(\frac{l_{c,d1}}{l_d y}\right)}{\frac{l_{c,d1}}{l_d y} - 1}}_{R_{D1}^{HD}}, \underbrace{\frac{\log_2\left(\frac{l_{c,d2}}{l_d x}\right)}{\frac{l_{c,d2}}{l_d x} - 1}}_{R_{HD}^{D2}}\right) \tag{54}$$

where R_{HD} $D1$ and R_{HD} $D2$ are the HD of $D1$ and $D2$ and they can be easily calculated by following the same procedure as in Lemma.1

7.3 Maximizing the full duplex D2D Ergodic capacity

The aim of this section is to maximize the FD-D2D capacity while satisfying the QoS requirement of the interferer CUE by finding the optimal power allocation scheme. Thus, the maximization problem denoted by $\boldsymbol{P}1$ can be formulated as,

$$\boldsymbol{P1}: \max_{\mathbf{P}} \quad R_{FD}(\mathbf{P}) = R_{D1} + R_{D2} \tag{55}$$

$$\text{s.t.} \quad \mathbb{E}[I_{BS}] \leq I^{\max} \tag{56}$$

where, $\mathbf{P} = [x = \frac{P_{d1}}{P_c}, y = \frac{P_{d2}}{P_c}]$ is the power ratio variable vector, $\mathbb{E}[I_{BS}]$ is the average interference power at eNodeB, and Imax denotes the maximum interference power that is acceptable at the BS. The utility function in (55) is the FD-D2D capacity presented in (50), while the constraint in (56) keeps the interference of the D2D users at a certain level and thus it reflects the QoS of the CUE. To obtain the optimal power allocation scheme, it is highly desirable that ***P***1 is a concave optimization problem. The next subsection will analyse the concavity of ***P***1.

7.3.1 Analysis of the full duplex rate

From (50-10), R_{FD} is defined if $y \neq \frac{l_{c,d1}}{l_d}$ and $x \neq \frac{l_{c,d2}}{l_d}$. Accordingly, the FD capacity is defined over four regions, $\mathcal{R}_1 = \{y < \frac{l_{c,d1}}{l_d}, x > \frac{l_{c,d2}}{l_d}\}$, $\mathcal{R}_2 = \{y > \frac{l_{c,d1}}{l_d}, x < \frac{l_{c,d2}}{l_d}\}$, $\mathcal{R}_3 = \{y < \frac{l_{c,d1}}{l_d}, x < \frac{l_{c,d2}}{l_d}\}$, and $\mathcal{R}_4 = \{y > \frac{l_{c,d1}}{l_d}, x > \frac{l_{c,d2}}{l_d}\}$

However, the main FD gain can only be achievable in $\mathcal{R}_4$. Otherwise, the FD gain will be less than 1bit/s/Hz. Intuitively, the FD gain is considerable in $\mathcal{R}_4$, where the average power of the useful signal is greater than the average interference power.

After further analysis, we found that the utility function (55-15) is concave in $\mathcal{R}_4$. On the other hand, to guarantee the QoS constraint on the CUE we need to ensure that the average interference power at the eNodeB is less than a predetermined threshold I^{max}. The average power of the useful signal received by the BS (i.e. the CUE signal) has been chosen as I^{max} .

$$\underbrace{\sum_{i=1}^{2} P_{di}\, l_{di,BS}\, h_{di,BS}}_{\mathbb{E}[I_{bs}]} \leq \underbrace{P_c l_{c,BS} h_{c,BS}}_{I^{\max}} \tag{57}$$

Moreover, it is straight forward to see that the maximum FD capacity rate occurs when the interference power of the D2D is at the maximum level (i.e. the equality case in ((57)). Now, solving (57) with equality leads to the following relation between the powers:

$$l_{c,BS} = l_{d1,BS}\, x + l_{d2,BS}\, y \tag{58}$$

where *x* and *y* are the power ratios defined in Theorem 1. As can be seen, (58) is linear. Thus, the problem ***P***1 is concave.

7.3.2 The Optimal power allocation scheme

Solving the derivative after applying (58) into (55) appears to be mathematically intractable and thus the optimum cannot be directly obtained. Therefore, we first split our problem into two sub-cases named symmetric and asymmetric scenarios. Then we solved the problem for the case where the interference power is much lower than the average received power, i.e. $y >> l_{c,d1}/l_d$ and $x >> l_{c,d2}/l_d$. Under this condition, we found out that the optimum of the symmetric case can be easily calculated by applying (58) into (55) and solving its derivative. The optimum in such case is :

$$x^*_{sym} = y^*_{sym} = \frac{l_{c,bs}}{2l_{d1,bs}} \tag{59}$$

Physically speaking, (59) means that when the D2D users are receiving the same interference power from CUE and introducing equal interference power at the BS, the optimum can be obtained by allocating half the maximum power for each D2D user. Moreover, (59) is true only when $\eta < l_d$. For the asymmetric case, the optimum is given by:

$$x^*{}_{asym} = \frac{A - \sqrt{B}}{2\eta e(el_{c,d1} - l_{c,d2})} \text{ and } y^*{}_{asym} = M - e\, x^*{}_{asym} \tag{60}$$

where, $M = l_{cbs}/l_{d2bs}$ is the maximum allowed power ratio for $D2$, $e = l_{d1,bs}/l_{d2,bs}$, $A = 4\eta e l_{c,d1} M + 3e l_{c,d1} l_{c,d2}$ and $B = A^2 - [(l_{c,d1} - l_{c,d2})(16M^2\eta^2 e l_{c,d1} + 24Me\eta l_{c,d1} l_{c,d2})]$. Proof: By using the properties of $E_1(z)$ given in [41] and assuming that the average received power is much larger than the interference power, R_{FD} can be written as follows:

$$R_{FD} \approx \ln(1 + \frac{l_d y}{\eta x}) + \ln(1 + \frac{l_d x}{\eta y}) - \ln(1 + \frac{l_{c,d1}}{\eta x}) - \ln(1 + \frac{l_{c,d2}}{\eta y}) \tag{61}$$

Now applying (58) into (61) and solving the derivative of the result leads to the optimum in (60). Moreover, after analysing (60) we found out that when the CUE is relatively far from the D2D pair, the optimum will be achieved by allocating more power to the D2D user which is introducing less interference power to the base station. While, when the CUE is relatively near the D2D pair, more power should be allocated to the D2D user which is suffering more from the

CUE interference power. Based on this analysis and the previous result, we propose the following closed form expression for the optimum in the general case:

$$x^* = \max(0, \min(M, e^{\frac{\eta M}{l_d}} \frac{M}{2} [1 + \frac{l_{c,d1} - l_{c,d2}}{l_d + l_{c,d1} + l_{c,d2}}]))$$
$$y^* = \frac{l_{c,bs} = l_{d1,bs} x^*}{l_{d2,bs}} \quad (62)$$

The max(.) and min(.) operators in (62) are used to ensure that our approximated optima does not violate the power ratio constrains i.e. the minimum power ratio 0 and the maximum power ratio M. The exponential term reflects the effect of the SIC techniques, more precisely when η goes to zero the effect of SI will disappear while when η goes to one the SI will highly affect the optimal solution. The fraction term in (62), will be positive or negative w.r.t the CUE location and thus more power will be allocated to *D*1 if he is suffering more from the CUE interference and vice versa. The accuracy of this approximation will be validated in the numerical results when comparing the derived optimal solution with the exhaustive search results.

7.4 Numerical results

In this section, we conduct numerical experiments to evaluate the performance of our proposed optimal power allocation model. For our simulation, we assume a circular cell of radius 500m. The maximum distance between the D2D users is assumed to be 40m as in [37][38]. Moreover, we set the path-loss exponent, α, to 3 and we varied the value of the SI mitigation factor η between two realistic values : -70dB and -90dB [33]-[38].

Figure 18 and Figure 19 validate the optimal power allocation for the symmetric and asymmetric cases respectively. For the symmetric case, we set the D2D pair 100m away from the eNodeB then we moved the CUE on the median line which intersects with the line *D*1 *D*2 in the triangle formed by the eNodeB, *D*1 and *D*2. In the asymmetric case, we fixed *D*1 100m away from the base station then we set *D*2 at a random position such that $d_{d2,bs} > d_{d1,bs}$ and $d_d \leq 40m$. Then, we set the CUE at a random position such that $d_{c,bs} < d_{d1,bs}$ and finally, we made CUE move toward *D*1. This scenario allows us to study the cases in which the CUE is close or far from D1 which in turn allows us to validate the power allocation strategy. The results obtained from our power allocation are very close to the exhaustive search results. Hence, the derived equations are valid and thus can be used to maximize the rate. In addition, from both Figure 18 and Figure 19 we can see that as η decreases, the FD rate increases.

The reason behind that is when η decreases the power of the residual self-interference decreases and hence the average interference power decreases. Moreover, both Figure 18 and Figure 19 shows that when the CUE is very close to one of the D2D user the maximum D2D capacity occurs by allocating the whole allowed power to that user. This is why all the curves in Figure 18 and Figure 19 converge to the same value as the interferer becomes closer to *D*1.

Now in order to show the high effect of the CUE location on the FD-D2D rate, first we fix the D2D pair 100m away from the BS. Then we set the CUE at a position where $d_{c,d1} > d_{c,d2}$. After that we moved the CUE toward *D*1 or *D*2. We have repeated this scenario for different values of l_d. Figure 20, shows the variation of the optimal powers with respect to the cellular user distances from the D2D users in such situation. As expected, x^* and y^* have opposite variation w.r.t the CUE location. For instance, when $d_{c,d1} = d_{c,d2}$, we have $x^* = y^* = 50$. While, when the CUE becomes too close to *D*1 (i.e. $d_{c,d1} = 5$), x^* is almost equal to the maximum allowed power ratio and y^* is almost zero. This is because in such case *D*1 is facing high interference from the CUE while *D*2 is not. Hence, it is better to let *D*1 only sends messages. Figure 21 shows the optimal rate variation with respect to $l_{c,d1}$ and $l_{c,d2}$. In addition, it compares the optimal FD rate with the optimal HD rate. As can be seen, the maximum FD gain occurs when $d_{c,d1} = d_{c,d2}$ while in the asymmetric case the FD rate decreases with the decrease of $d_{c,d1}$ or $d_{c,d2}$. Hence, when the CUE is too close to one of the D2D users the FD has no rate gain. Finally, Figure 21 clearly shows that the FD rates decreases with the increase of the D2D distance.

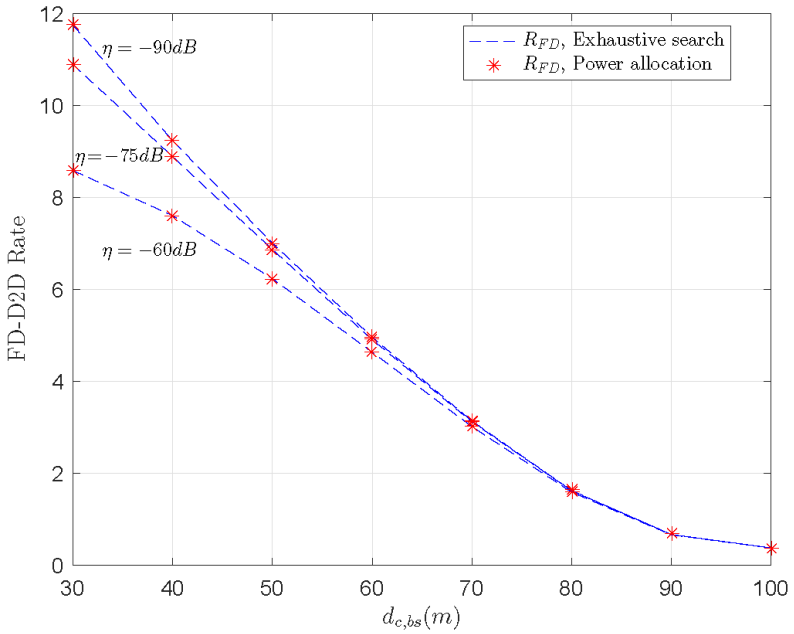

Figure 18: Comparison of FD-D2D rate obtained from the exhaustive search and from the proposed power allocation scheme in the symmetric case

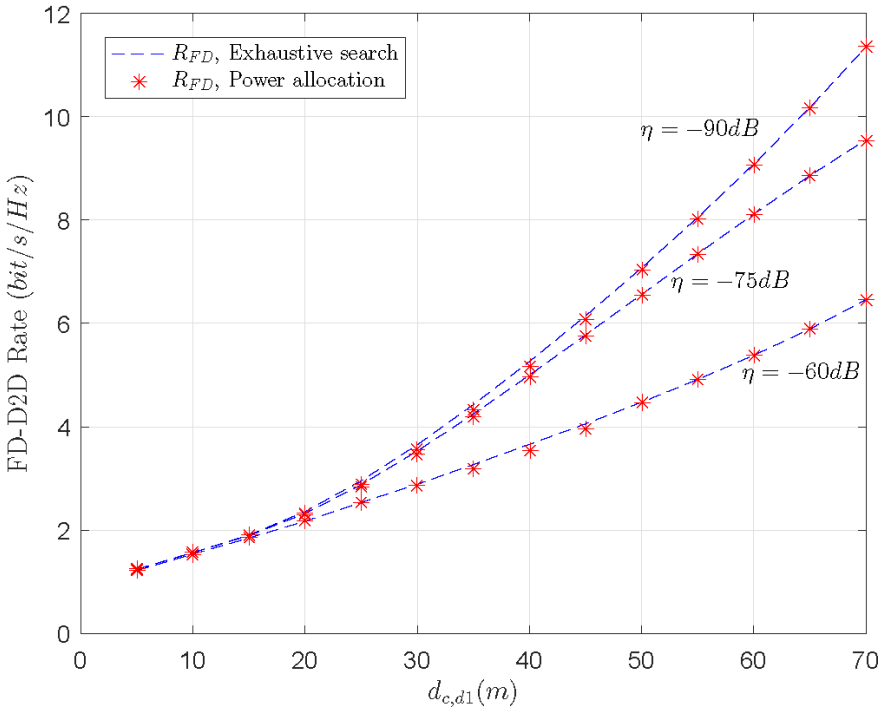

Figure 19: Comparison of FD-D2D rate obtained from the exhaustive search and from our proposed power allocation scheme in the asymmetric case

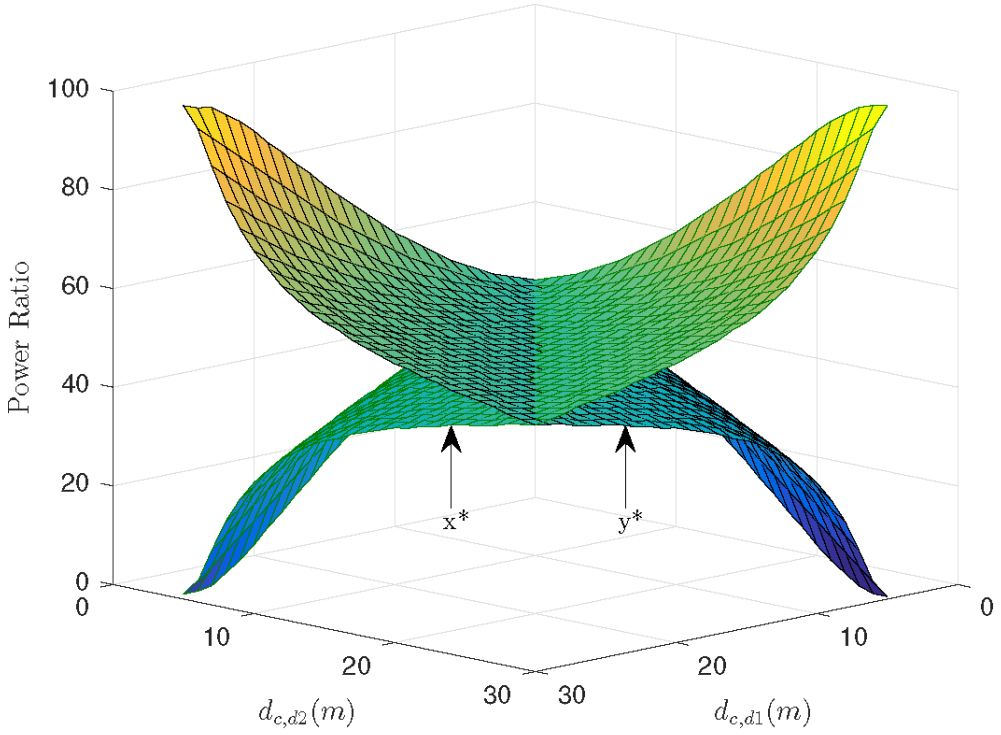

Figure 20: The optimal power ratios variation w.r.t to CUE location.(η =-70dB)

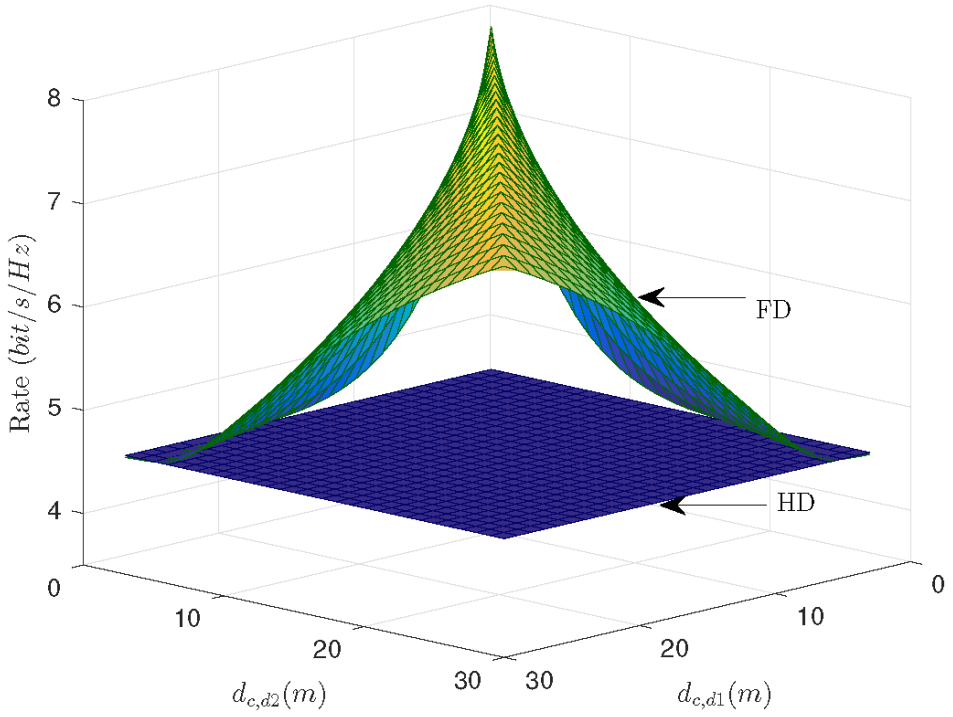

Figure 21: The effect of the CUE location on the FD rate.(η = -70dB)

7.5 Main outputs

In the Section 7, we have investigated the power allocation problem for FD-D2D based cellular network. In particular, we formulated an optimization problem to maximize the FD-D2D rate while fulfilling the minimum QoS requirement of CUE. We further derived a closed-form expression for the optimal power allocation strategy. On contrary to the related

works, the derived solution covered both the symmetric and the asymmetric scenarios. The simulation results proved the derived equation and showed that the distance from the interferer cellular user, the distance between the D2D pair, and the SIC factor have a great impact on the FD-D2D ergodic capacity and the power allocation scheme. For instance, when CUE is relatively far from the D2D pair the optimum will be achieved by allocating more power to the D2D user who is introducing less interference power to the base station. While when the CUE is relatively near the D2D pair, more power should be allocated to the D2D user who is suffering more from the CUE interference power. Finally, both simulation and analysis showed that the maximum FD-D2D rate occurs when the D2D users are sharing the CUE spectrum which is located near the BS and far from the D2D pair. As a result, the user location or in general the user interference highly affects the D2D rate and thus, it should be well treated in the resource allocation phase.

8 Conclusion

This deliverable has provided a framework of resource allocation algorithms for D2D asynchronous communications. A efficient way of writing resource allocation problems while taking into account ICI and per-Resource Block power allocation has first been provided. Then a distributed power allocation algorithm aiming at maximizing the weighted sum rate of D2D pairs, under the underlay Base Station interference constraint, has been detailed. The Resource Block allocation problem has also been considered, with the objective to maximize the average multiplexing ratio. Simulation results show that FBMC-OQAM is always more efficient than CP-OFDM in D2D asynchronous communications, whatever the tested algorithm. These results could be even better if we used a new waveform, called COW-CFMC, that is presented in details in this deliverable. This waveform is shown to be very robust to time and frequency misalignment. Consequently, it is very likely to provide even better results than FBMC-OQAM for D2D communications.
Moreover, the influence of the coexistence of various waveforms such as FBMC, UFMC, FMT, GFDM and OFDM in asynchronous transmissions has been provided and evaluated with system-level simulations. The obtained results showed that with several enhanced waveforms, D2D pairs can achieve high data rate while coexisting with cellular users.
Finally, this deliverable has investigated the influence of Full Duplex devices for D2D communications, where all devices can transmit and receive at the same time. Taking into account self-interference, the ergodic capacity was derived, and an algorithm to maximize the ergodic capacity by optimizing power allocation was proposed. We showed that the ergodic capacity improvement thanks to FD depend on the relative location of D2D and of the interference cellular users that share the same frequency resources, as well as on the ability of devices to remove self-interference.

9 References and glossary

9.1 References

[1] H. Lin and P. Siohan, “Multi-carrier modulation analysis and WCP-COQAM proposal,”EURASIP J. Appl. Signal Process., vol. 2014, no. 1, pp. 1–19, May. 2014.

[2] R. Zakaria, D. Le Ruyet, C. A. F. da Rôcha and B. F. U. Filho, "A complex orthogonal WCP circular filtered multi-carrier (COW-CFMC) scheme," *2017 IEEE International Conference on Communications (ICC)*, Paris, 2017, pp. 1-6.

[3] M. J. Abdoli, M. Jia, and J. Ma. Weighted circularly convolved filtering in OFDM/OQAM. In 2013 IEEE 24th Annual International Symposium on Personal, Indoor, and Mobile Radio Communications (PIMRC), pages 657–661, Sept 2013.

[4] G. Fettweis, M. Krondorf, and S. Bittner. GFDM - Generalized Frequency Division Multiplexing. In Vehicular Technology Conference, 2009. VTC Spring 2009. IEEE 69th, pages 1–4, April 2009.

[5] P. Siohan, C. Siclet, and N. Lacaille. Analysis and design of OFDM/OQAM systems based on filterbank theory . Signal Processing, IEEE Transactions on, 50(5):1170 –1183, may 2002.

[6] A. I. Pérez-Neira, M. Caus, R. Zakaria, D. Le Ruyet, E. Kofidis, M. Haardt, X. Mestre, and Y. Cheng. MIMO Signal Processing in Offset-QAM Based Filter Bank Multicarrier Systems. IEEE Transactions on Signal Processing, 64(21):5733–5762, Nov 2016.

[7] Rostom Zakaria, Didier Le Ruyet, Intrinsic interference reduction in a filter bank-based multicarrier using QAM modulation, In Physical Communication, Volume 11, 2014, Pages 15-24, ISSN 1874-4907.

[8] R. Zakaria and D. Le Ruyet. A novel FBMC scheme for Spatial Multiplexing with Maximum Likelihood detection. In Wireless Communication Systems (ISWCS), 2010 7th International Symposium on ,pages 461 – 465, sept. 2010.

[9] R. Zakaria and D. Le Ruyet. A Novel Filter-Bank Multicarrier Scheme to Mitigate the Intrinsic Interference: Application to MIMO Systems. IEEE Transactions on Wireless Communications,, 11(3):1112 –1123, march 2012.

[10] S. Mirabbasi and K. Martin. Design of prototype filter for near-perfect-reconstruction overlapped complex-modulated transmultiplexers. In . IEEE International Symposium on Circuits and Systems ISCAS 2002, volume 1, pages I–821–I–824 vol.1, 2002.

[11] Y. Medjahdi, M. Terre, D. Le Ruyet, D. Roviras, J.A. Nossek and L. Balter, “Inter-cell interference analysis of OFDM/FBMC systems”, *in Proc. SPAWC*, Perugia, Italy, June 2009.

[12] S. Boyd and L. Vandenbergue, “Convex optimization”, Cambridge, UK: Cambridge University Press, 2004.

[13] J. Huang, R.A. Berry and M.L. Honig, “Distributed interference compensation for wireless networks”, *IEEE Journal on Selected Areas in Communications*, vol.24, no.5, pp. 1074-1084, May 2006.

[14] Guidelines for evaluation of radio transmission technologies for IMT 2000, doc. Rec. ITU-R, M.1225, 1997.

[15] D. Brélaz, “New methods to color the vertices of a graph”, *Commun. ACM*, vol.22, no.4, pp.251-256, April 1979.

[16] M. Pischella and J-C. Belfiore, « Distributed resource allocation for rate-constrained users in multi-cell OFDMA networks », IEEE Communication Letters, vol. 12, no. 4, pp. 250-252, April 2008.

[17] C. Sexton, Q. Bodinier, A. Farhang, N. Marchetti, F. Bader, and L. A. DaSilva, “Coexistence of OFDM and FBMC for Underlay D2D Communication in 5G Networks,” in Proc. of 2016 IEEE Global Communications Conference Workshops (Globecom Wkshps), Washington D.C., Dec. 2016, pp. 1–7.

[18] Q. Bodinier, A. Farhang, F. Bader, H. Ahmadi, J. Palicot, and L. A. DaSilva, “5G Waveforms for Overlay D2D Communications: Effects of Time-Frequency Misalignment,” in Proc. of 2016 IEEE International Conference on Communications (ICC), Kuala Lumpur, May 2016.

[19] Y. Medjahdi, M. Terré, D. Le Ruyet, and D. Roviras, “Interference tables: a useful model for interference analysis in asynchronous multicarrier transmission,” EURASIP Journal on Advances in Signal Processing, vol. 2014, no. 54, pp. 1–17, Apr. 2014.

[20] Q. Bodinier, F. Bader, and J. Palicot, "Modeling Interference Between OFDM / OQAM and CP-OFDM : Limitations of the PSD-Based Model," in Proc. of 2016 International Conference on Telecommunications (ICT), Thessaloniki, May 2016.

[21] N. Saquib, E. Hossain, and D. Kim, "Fractional frequency reuse for interference management in LTE-advanced hetnets," IEEE Wireless Communications, vol. 20, no. 2, pp. 113–122, Apr. 2013.

[22] T. Novlan, J. G. Andrews, I. Sohn, R. K. Ganti, and A. Ghosh, "Comparison of Fractional Frequency Reuse Approaches in the OFDMA Cellular Downlink," in Proc. of 2010 IEEE Global Communications Conference (Globecom). Miami: IEEE, Dec. 2010, pp. 1–5.

[23] H. Xing and M. Renfors, "Investigation of filter bank based deviceto-device communication integrated into OFDMA cellular system," in Proc. of the 11th International Symposium on Wireless Communications Systems (ISWCS), Barcelona, Aug. 2014, pp. 513–518.

[24] K. Doppler, M. Rinne, C. Wijting, C. B. Ribeiro, and K. Hugl, "Deviceto-device communication as an underlay to LTE-advanced networks," IEEE Communications Magazine, vol. 47, no. 12, pp. 42–49, Dec. 2009.

[25] C.-H. Yu, K. Doppler, C. B. Ribeiro, and O. Tirkkonen, "Resource Sharing Optimization for Device-to-Device Communication UnderlayingCellular Networks," IEEE Transactions on Wireless Communications, vol. 10, no. 8, pp. 2752–2763, Aug. 2011.

[26] P. Kyösti, J. Meinilä, L. Hentilä, X. Zhao, T. JämsPa, C. Schneider, M. Narandzic, M. Milojevic, A. Hong, J. Ylitalo et al., "WINNER II channel models," WINNER II Public Deliverable, pp. 42–44, 2007.

[27] "LTE; Evolved Universal Terrestrial Radio Access (E-UTRA); Radio Frequency (RF) system scenarios", 3GPP, Tech. Rep. TR 36.942 V14.0.0, Apr. 2017.

[28] ACCENT5 project, deliverable D1.2 "Advanced FB-MC for D2D Communications, Technical report Jan. 2017

[29] Quentin Bodinier, Faouzi Bader, Jacques Palicot, "On Spectral Coexistence of CP-OFDM and FB-MC Waveforms in 5G Networ**ks**", IEEE Access Journal (Volume 5), pp. 13883 – 13900, doi: 10.1109/ACCESS.2017.2723822. July 2017.

[30] A. A. Al Haija and M. Vu, "Spectral efficiency and outage performance for hybrid d2d-infrastructure uplink cooperation," IEEE Transactions on Wireless Communications, vol. 14, no. 3, pp. 1183–1198, 2015.

[31] Z. Zhang, K. Long, A. V. Vasilakos, and L. Hanzo, "Full-duplex wireless communications: challenges, solutions, and future research directions," Proceedings of the IEEE, vol. 104, no. 7, pp. 1369–1409, 2016.

[32] A. Sabharwal, P. Schniter, D. Guo, D. W. Bliss, S. Rangarajan, and R. Wichman, "In-band full-duplex wireless: Challenges and opportunities," IEEE Journal on Selected Areas in Communications, vol. 32, no. 9, pp. 1637–1652, 2014.

[33] K. E. Kolodziej, J. G. McMichael, and B. T. Perry, "Multitap rf canceller for in-band full-duplex wireless communications," IEEE Transactions on Wireless Communications, vol. 15, no. 6, pp. 4321–4334, 2016.

[34] L. Laughlin, C. Zhang, M. A. Beach, K. A. Morris, and J. Haine, "A widely tunable full duplex transceiver combining electrical balance isolation and active analog cancellation," in 2015 IEEE 81st Vehicular Technology Conference (VTC Spring), May 2015, pp. 1–5.

[35] V. Tapio, "System scenarios and technical requirements for full-duplex concept," DUPLO, Project Deliverable, 2013.

[36] W. Cheng, X. Zhang, and H. Zhang, "Optimal power allocation for fullduplex d2d communications over wireless cellular networks," in 2014 IEEE Global Communications Conference, Dec 2014, pp. 4764–4769.

[37] B. Zuo, L. Jiang, C. He, and Z. Lian, "Power allocation optimization for full-duplex d2d communications underlaying cellular networks," in 2016 International Conference on Networking and Network Applications (NaNA). IEEE, 2016, pp. 103–108.

[38] S. Dang, G. Chen, and J. P. Coon, "Outage performance analysis of full-duplex relay-assisted device-to-device systems in uplink cellular networks," IEEE Transactions on Vehicular Technology, vol. 66, no. 5, pp. 4506–4510, 2017.

[39] X. Chai, T. Liu, C. Xing, H. Xiao, and Z. Zhang, "Throughput improvement in cellular networks via full-duplex based device-to-device communications," IEEE Access, vol. 4, pp. 7645–7657, 2016.

[40] V. Raghavan, S. V. Hanly, and V. V. Veeravalli, "Statistical beamforming on the grassmann manifold for the two-user broadcast channel," IEEE Transactions on Information Theory, vol. 59, no. 10, pp. 6464–6489, 2013.

[41] M. Abramowitz and I. A. Stegun, Handbook of Mathematical Functions with Formulas, Graphs and Mathematical Tables, 10th ed. Gaithersburg, MD, USA: National Bureau of Standards, 1972.

[42] S. Boyd and L. Vandenberghe, Convex Optimization. Cambridge University press, 2004.

[43] R. A. Horn and C. R. Johnson, Matrix Analysis. Cambridge University press, 2012.

9.2 Glossary

D2D	*Device to device*	
UL	*Uplink*	
DL	*Downlink*	
FDD	*Frequency division duplex*	
TDD	*Time division duplex*	
FBMC	*Filter Bank Multicarrier*	
OFDM	*Orthogonal frequency-division multiplexing*	
RB	*Resource block*	
CP-OFDM	*Cyclic Prefix Orthogonal frequency-division multiplexing*	
TS	*Time slot*	
DUE	*D2D user equipment*	
CUE	*Cellular user equipment*	
BS	*Base Station*	
LTE	*Long term evolution*	
TO	*Timing Offset*	
SNR	*Signal over noise ratio*	
SINR	*Signal over interference plus noise ratio*	
FFR	*Fractional Frequency Reuse*	
OFDMA	*Orthogonal frequency-division multiple Access*	
COW-CFMC	*Complex Orthogonal Windowed Cyclic Prefix circular filtered multi-carrier*	
GFDM	*Generalized Frequency Division Multiplexing*	
WCP/COQAM	*Windowed Cyclic Prefix Circular Offset Quadrature Amplitude Modulation*	
COQAM	*Circular Offset Quadrature Amplitude Modulation*	
FFT FBMC	*Fast Fourier Transform Filter Bank Multicarrier*	
STBC	*Space Time Block Code*	
MIMO	*Multiple Input, Multiple Output*	
SM-ML	*Spatial Multiplexing with Maximum Likelihood*	
NMSE	*Normalized Mean Error Square*	
CFO	*Carrier Frequency Offset*	
CP	*Cyclic Prefix*	
FMT	*Filtered MultiTone*	
FBMC-PAM	*Orthogonal frequency-division multiplexing- Pulse Amplitude Modulation*	
UFMC	*Universal Filtered Multi-Carrier*	
F-OFDM	*Filtered OFDM*	